Cite this article as: Nomura M., et al. (2024). Ketogenic Diet Reduces Age-Induced Chronic Neuroinflammation in Mice, *AgingBio*, *2*, e20240038. doi: 10.59368/agingbio.20240038.

Research Paper

Ketogenic Diet Reduces Age-Induced Chronic Neuroinflammation in Mice

Mitsunori Nomura,[1] Natalia Faraj Murad,[1] Sidharth S. Madhavan,[1,2] Wei-Chieh Mu,[1] Brenda Eap,[1,2] Thelma Y. Garcia,[1] Carlos Galicia Aguirre,[1,2] Eric Verdin,[1] Lisa Ellerby,[1,2] David Furman[1,3,4] and John C. Newman[1,2,5,*]

[1]Buck Institute for Research on Aging, Novato, CA, USA
[2]Leonard Davis School of Gerontology, University of Southern California, Los Angeles, CA, USA
[3]Stanford 1000 Immunomes Project, Stanford University School of Medicine, Stanford, CA, USA
[4]Instituto de Investigaciones en Medicina Traslacional, Universidad Austral, Consejo Nacional de Investigaciones Científicas y Técnicas, 1629, Pilar, Argentina
[5]Division of Geriatrics, University of California, San Francisco, CA, USA
[*]Corresponding author: jnewman@buckinstitute.org
https://doi.org/10.59368/agingbio.20240038
Received: 12/4/2023, Revised: 8/28/2024, Accepted: 11/16/2024, Published: 12/16/2024

The ketone body beta-hydroxybutyrate (BHB) is an acidic energy metabolite that is synthesized during periods of fasting or exercise. Our previous study demonstrated that an every other week cyclic ketogenic diet (Cyclic KD), which induces blood BHB levels similar to those observed during fasting, reduces midlife mortality and improves memory in aging mice. In addition to its canonical role as an energy metabolite, BHB regulates gene expression and inflammatory activation through non-energetic signaling pathways. The precise mechanisms by which BHB or KD affects brain function during aging remain incompletely understood. Using bulk RNA-sequencing (RNA-Seq), we examined whole brain gene expression of 12-month-old C57BL/6JN male mice fed KD for either one week or 14 months. While one-week KD increases some inflammatory gene expression, the 14-month Cyclic KD largely reduces age-induced neuroinflammatory gene expression. Next, a gene expression analysis of human primary brain cells (microglia, astrocytes, and neurons) using RNA-Seq revealed that BHB alone induces a mild level of inflammation in all three cell types. However, BHB inhibits the more pronounced inflammatory gene expression induced by lipopolysaccharide (LPS) in microglia. BHB exhibits a comparable inhibitory effect on LPS-induced inflammation in mouse primary microglia, which we used as an *in vitro* model to test and exclude known mechanisms by which BHB regulates inflammation and gene expression as responsible for this modulation of LPS-induced inflammatory gene expression. An acidic milieu resulting from BHB may be required for or contribute to the effect. Overall, we observe that BHB has the potential to attenuate the microglial response to inflammatory stimuli, such as LPS. This may contribute to an observed reduction in chronic inflammation in the brain following long-term Cyclic KD treatment in aging mice.

Introduction

The ketone body beta-hydroxybutyrate (BHB) is a small acidic metabolite primarily synthesized in the liver that functions as a glucose-sparing energy source for extrahepatic organs, including the brain and heart[1–3]. In healthy adults, the non-fasting blood concentration ranges from 0.05 to 0.25 mM, while with prolonged exercise or fasting, or the absence of dietary carbohydrates, it can reach 0.5–8 mM[2]. In addition to its role as an energy metabolite, BHB is increasingly recognized as a signaling molecule[2]. For instance, it acts as an inhibitor of the NLRP3 inflammasome[4,5], an inhibitor of class I histone deacetylases (HDACs)[6], and also a substrate for the protein posttranslational modification lysine beta-hydroxybutyrylation (Kbhb)[7]. Moreover, BHB serves as a ligand for the G protein-coupled receptor (GPCR) hydroxycarboxylic acid receptor 2 (HCAR2, HCA2, GPR109A)[8]. A recent study found that BHB can prevent vascular senescence by binding to heterogeneous nuclear ribonucleoprotein A1 (hnRNP A1), a member of the hnRNP family responsible for RNA processing, and thereby enhancing the expression of *Oct4*[9]. The two enantiomers of BHB are designated as R-BHB and S-BHB. The former is the endogenous ketone body and can be readily catabolized into acetyl-CoA and adenosine triphosphate (ATP), whereas the latter is a by-product of fatty acid metabolism that cannot be metabolized through the ketone body oxidation pathway[2]. A ketogenic diet (KD) is a macronutrient diet pattern that consists primarily of fats with moderate amounts of protein and little to no carbohydrate in order to promote endogenous ketone body production. High-fat diets that are not ketogenic result in obesity and a range of associated deleterious phenotypes in mice[10], so dissociating the effects of diet-induced obesity from KD is important for interpreting the effects of KD in aging. In the short term, *ad libitum* KD feeding largely does not result in obesity in mice. One study showed that two distinct

three-week *ad libitum* KD regimens did not result in body weight gain[11]. Another study demonstrated that *ad libitum* KD can result in a reduction in body weight within a two-week period[12]. However, the long-term effects of KD on body weight in mice have been observed to vary considerably across different studies.

One recent report found that a seven-week *ad libitum* KD resulted in a 40% reduction in body weight and demonstrated metabolic benefits[13]. In contrast, Goldberg *et al.* demonstrated that a four-month *ad libitum* KD resulted in a significant increase in body weight and metabolic dysfunction[14]. Our group and Ang *et al.* also reported a significant body weight gain by continuously fed, *ad libitum* KD[15,16]. The composition of KD varies across studies, making it challenging to draw generalizable conclusions about the effects of KD on mice. For example, some studies use a KD formulated with a protein ratio significantly lower than that of a standard control diet (CD), which may confound the effects of KD given the pivotal role of protein restriction in weight loss[17] and aging[18]. As is the case with humans[19], the composition, duration, periodicity, and feeding pattern of a KD regimen can all alter its effect on obesity.

Two recent studies used different techniques to provide long-term exposure to KD without obesity in order to test the effect of KD on mouse lifespan and healthspan. Roberts *et al.* showed that daily fixed-calorie feeding of KD enhances longevity and healthspan, including improved memory, in aging mice[20]. In our study, long-term continuous *ad libitum* KD (with a protein ratio equivalent to that of CD) resulted in a significant increase in both mortality and body weight, whereas every other week "Cyclic" KD, where KD is alternated with CD, prevented obesity and resulted in reduced mortality and improvements in memory in aging mice[15]. Recently, Tomita *et al.* demonstrated that feeding aging mice with the exogenous BHB precursor 1,3-butanediol (1,3-BD) increases lifespan[21], and the National Institute of Aging (NIA)-supported Interventions Testing Program (ITP) found that 1,3-BD increased lifespan in both male[22] and female[23] mice, though with nonuniform effects across the lifespan. Although the physiological effects of KD are pleiotropic[24] and 1,3-BD has an antiaging role that is independent of BHB[25], the findings of these studies suggest that the direct promotion of BHB production by KD may have the potential to enhance lifespan and healthspan in aging mice. Nevertheless, the precise mechanisms by which this occurs remain unclear. One possibility is via regulation of target of rapamycin (TOR) signaling, a pathway known to broadly regulate longevity, both in the setting of pharmacological inhibition and when inhibited via caloric restriction[26]. The TOR pathway responds to nutrients (e.g., glucose, amino acids) and, in turn, regulates protein synthesis, autophagy, and lipid metabolism[27]. Rapamycin, a TOR inhibitor, extends the lifespan of various strains of mice[28]. In our previous study, we conducted RNA-sequencing (RNA-Seq) and quantitative PCR (qPCR) analyses of liver and kidney tissue and found that both one-week KD and 14-month Cyclic KD reduced TOR activation and upregulated peroxisome proliferator-activated receptor alpha (PPARα) target genes[15]. Roberts *et al.* also found that long-term KD inhibits hepatic TOR signaling[20]. Although both studies indicate that long-term KD improves memory in the aging brain, neither explored the transcriptional changes induced by KD in the brain or any cell-specific effects of BHB in the brain. In this study, we first examined whole brain gene expression in our long-term KD cohort[15] and found that the 14-month Cyclic KD intervention reduces age-induced neuroinflammatory gene expression in 26-month-old mice. Then, using *in vitro* models, we show that R-BHB modestly activates inflammatory pathways in human primary astrocytes and neurons but suppresses the potent pro-inflammatory gene expression patterns induced by LPS in primary human and mouse microglia.

In summary, long-term Cyclic KD reduces age-induced neuroinflammation *in vivo* and BHB decreases LPS-induced inflammation in microglia *in vitro*, supporting a key role for inflammatory modulation in the effect of KD on ameliorating brain aging phenotypes in mice.

Materials and Methods

Mouse strains, housing, and husbandry

The mouse experiments involved mice housed either at Buck Institute for primary cell isolation or, for long-term Cyclic KD studies, mice formerly housed at Gladstone Institutes (as previously described[15]). All mice were maintained according to the National Institutes of Health guidelines, and all experimental protocols were approved by the Buck Institute Institutional Animal Care and Use Committee (IACUC) or the University of California, San Francisco (UCSF) IACUC (for mice previously housed at Gladstone). All mice were maintained in a specific pathogen-free barrier facility on a 6:00 a.m. to 6:00 p.m. light cycle (7:00 a.m. to 7:00 p.m. at Gladstone). Specific information on the sex, age, diet, and time course of all mice used in the *in vivo* RNA-Seq and immunophenotyping experiments has been described previously[15]. Briefly, C57BL/6JN male mice were obtained from the NIA Aged Rodent Colonies at 11 months of age and started on experimental diets at 12 months of age. Aging mice were monitored with increasing frequency based on a protocol developed in collaboration with UCSF Laboratory Animal Resource Center veterinarians. The groups of mice designated for tissue collection after one week and 14 months on the experimental diets were separate from the other lifespan and behavioral testing cohorts[15]. Mice that had been fed Cyclic KD were switched to CD five days prior to the time of their euthanasia and tissue collection. To prepare primary microglia, astrocytes, and bone marrow-derived macrophages (BMDMs), we initially acquired C57BL/6JN mice from the NIA Aged Rodent Colonies.

Mouse diets and feeding

Details of the mouse experimental diets have been previously described[15]. Upon arrival, until switched to experimental diets, mice were fed the Gladstone Institute's standard vivarium chow with 24% protein, 13% fat, and 62% carbohydrates. The customized diets from Envigo contained the following macronutrient content per calorie: CD with 10% protein, 13% fat, and 77% carbohydrate (TD.150345); KD with 10% protein and 90% fat (TD.160153). Both diets had similar micronutrient content, fiber, and preservatives on a per-calorie basis, had similar fat sources, and were always provided *ad libitum*. All food was changed once per week; for the Cyclic KD condition, this involved switching diets.

RNA-Seq

The liver RNA-Seq dataset from the one-week KD cohort has already been published[15]. For the new *in vivo* RNA-Seq, RNA was isolated using the Direct-zol RNA MiniPrep kit (R2052; Zymo Research) following the manufacturer's protocol. Subsequent RNA sample processing was conducted by the University of California, Davis (UC Davis) DNA Technologies & Expression Analysis Core. RNA integrity and concentrations were assessed using an Agilent Bioanalyzer. The library was prepared using

the KAPA RNA HyperPrep Kit (KK8541; Roche) and QIAseq FastSelect Custom RNA Removal Kit (333390; QIAGEN), and sequencing was performed on a NovaSeq 6000 (Illumina). For the *in vitro* (3' Tag-Seq) RNA-Seq experiments, RNA was isolated using the Quick-RNA MicroPrep Kit (R1051; Zymo Research) according to the manufacturer's protocol. Downstream processing of the RNA samples was carried out by the UC Davis DNA Technologies & Expression Analysis Core. RNA integrity and concentrations were confirmed using an Agilent Bioanalyzer. The library was prepared with the KAPA RNA HyperPrep Kit and sequenced on a HiSeq 4000 (Illumina). Quality reports were assessed before and after trimming reads using FastQC (http://www.bioinformatics.babraham.ac.uk/projects/fastqc/) and MultiQC (https://multiqc.info). During data processing, low-quality bases and adapters were removed using Trimmomatic, and reads were mapped to the reference genome (GRCm38; http://nov2020.archive.ensembl.org/Mus_musculus/Info/Index) with STAR[29,30]. The count matrices were generated with RSEM[31]. For differential expression analysis, DEseq2 was used[32], and p-values were corrected using the false discovery rate (FDR) method. We defined differentially expressed genes (DEGs) as those with FDR-adjusted p-value < 0.05 and $|\log_2$ fold change$| > 1.0$. The panther database was used for transcript annotation[33]. Enrichment analyses to find significant pathways/signatures associated with the DEGs were done using clusterprofiler[34,35], DOSE[36], org.Hs.eg.db[37], and org.Mm.eg.db[38]. Data were visualized using packages ggplot2[39] and gridExtra. Gene lists were prepared for gene set enrichment analysis (GSEA)[40] by ranking by t-statistic, and duplicate or missing gene identifiers were removed. We used the Molecular Signatures Database (MSigDB) hallmark gene set[41], gene ontology (GO)[42], and Kyoto Encyclopedia of Genes and Genomes (KEGG)[43] for additional enrichment analyses. To perform the correlation analyses, gene ranks were calculated via the following equation: corr * (−1) * log10(p-value). Subsequently, the ranked list was used for the MSigDB hallmark gene set. GSEA for the GO biological process was executed for genes with an adjusted p-value cutoff of 0.01 and GSEA for the KEGG pathway was executed for genes with an adjusted p-value cutoff of 0.05. To visualize concordant and discordant gene overlap, the Rank–Rank Hypergeometric Overlap (RRHO) package was used[44]. We selected the lists of common genes between the pairs of comparisons and generated separate lists of down- and upregulated genes. We ordered all the genes by $\log_2$ fold change and generated the gene lists that provided the most significant overlap. Cell fractions of bulk RNA-Seq were imputed by CIBERSORTx as described[45]. The single-cell reference was the normalized count matrix derived from the young samples of the single-nucleus RNA-Seq data from Ogrodnik *et al.*[46] To generate the normalized count matrix, the cell ranger output was downloaded from GSE161340, and data preprocessing, dimensionality reduction, and clustering were performed via Scanpy (v. 1.9.5)[47]. Cluster identities were assigned by the following marker genes: *Plp1* and *Mbp* for oligodendrocytes; *Syt1* for neurons; *Syt1*, *Egfr*, and *Igf1* for interneurons; *Slc6a13* for vascular and leptomeningeal cells; *Gja1* and *Aldoc* for astrocytes; *C1qa*, *C1qb*, and *Hexb* for microglia; and *Pdgfra* for oligodendrocyte precursor cells. Imputation of cell fractions was done by the default settings of the CIBERSORTx program with 100 permutations for p-value calculation.

Flow cytometry

Following blood collection, red blood cells were lyzed using an ammonium-chloride-potassium buffer. Lymphocytes from the blood were stained with the LIVE/DEAD Fixable Green Dead Cell Stain Kit (L34970; Invitrogen) and antibodies against the following surface antigens: TCRβ (H57-597, BioLegend), CD4 (RM4-5, BioLegend), CD8 (53-6.7, BioLegend), and PD-1 (J43; BD Biosciences), then fixed with 1% PFA. For FOXP3 staining, the cells underwent an additional staining process using anti-FOXP3 (MF23; BD Biosciences), following the manufacturer's protocol. Stained cells were acquired on a BD LSR II Flow Cytometer (BD Biosciences), and FlowJo software (BD Biosciences) was used for data analysis.

Cell culture

Human primary microglia (Cat. No. 1900), astrocytes (Cat. No. 1800), and neurons (Cat. No. 1520) were purchased from ScienCell. No identifying information such as sex, age, or origin of the cells was provided. The culture media were Microglia Medium (Cat. No. 1901), Astrocyte Medium (Cat. No. 1801), and Neuron Medium (Cat. No. 1521), respectively (all include 10% fetal bovine serum (FBS), penicillin-streptomycin, and growth supplement). For preparation of mouse primary microglia and astrocytes, we followed a standard protocol with modifications[48]. C57BL/6JN newborn pups (postnatal days 0–2) were euthanized by decapitation. The brains were collected and triturated in PBS using a 5 ml serological pipette. After centrifugation, cells were resuspended and plated in poly-L-lysine-coated flasks. The cells were cultured in DMEM (10-013-CV; Corning) with 10% FBS (35-011-CV; Corning) and penicillin-streptomycin (30-002-CI; Corning), and the medium was replaced at least two to three times per week. After ten days, microglia were removed and collected by tapping and shaking the flasks. The remaining cells in the flasks were used as astrocytes. Both IMG and BV-2 cells were kindly provided by the Andersen Lab at the Buck Institute and cultured in DMEM with 10% FBS and penicillin-streptomycin. For the preparation of BMDMs, we followed a standard protocol with modifications[49]. Adult C57BL/6JN mice were euthanized, and the leg bones were cleaned. The bone marrow was flushed from the bones using PBS. The cells were then centrifuged, resuspended, and plated on Petri dishes. The cells were cultured in DMEM with 10% FBS, penicillin-streptomycin, and 10 ng/ml of M-CSF (576404; BioLegend). New medium was added three days later, and after seven days, macrophages were collected for subculturing. Cells were treated with 10 mM (or 1 or 5 mM in **Supplemental Fig. 16B**) R-BHB (54920; Sigma), 10 mM S-BHB (54925; Sigma), 10 mM Na-R-BHB (298360; Sigma), 10 mM Na-S-BHB (sc-236887; Santa Cruz), 5 mM Bu (L13189; Alfa Aesar), 5 mM Na-Bu (B5887; Sigma), 100 ng/ml LPS (sc-3535; Santa Cruz), 10 mM sodium chloride (NaCl; BDH9286; VWR), 6.75 mM (or 3.75 mM in **Supplemental Fig. 18D**) sodium hydroxide (NaOH; BDH7247-1; VWR), 15 mM hydrochloric acid (HCl; BDH7418-1; VWR), 5 mM ATP (tlrl-atpl; InvivoGen), 10 μM nigericin (tlrl-nig; InvivoGen), 1 μM MCC950 (17510; Cayman), 150 μM hydrogen peroxide (H_2O_2; 868170; Carolina), or 300 μM arachidonic acid (AA; A3611; Sigma), following the schemes and time course described in the figures and text. A standard protocol is employed for the induction of senescence via ionizing radiation (IR)[50], in which cells were irradiated with 15 gray (Gy) one hour after pre-incubation with R-BHB, and the medium was changed daily.

Measurement of oxygen consumption

The oxygen consumption of the cells was quantified using a Seahorse XF96 Analyzer (Agilent Technologies). Mouse primary

microglia were cultured in 96-well Seahorse plates in the culture medium. The assay was then performed in unbuffered DMEM (pH 7.4) containing 1.8 mM $CaCl_2$, 139 mM NaCl, 20 mM HEPES, 1 mM $NaHCO_3$, 25 mM glucose, 1 mM pyruvate, and 4 mM glutamine. The respiratory rate was quantified in eight five-minute intervals. Initially, 2.5 μM (final concentration) oligomycin (O4876; Sigma) was added to assess the coupling efficiency. Maximal respiration was quantified with the addition of 1.5 μM (final concentration) carbonyl cyanide 4-(trifluoromethoxy)phenylhydrazone (C2920; Sigma). Subsequently, 2.5 μM (final concentration) antimycin A (A8674; Sigma) was added.

Small interfering RNA (siRNA) transfection

Three synthetic siRNAs, siGENOME Non-Targeting siRNA Control Pool #1 (siCtrl; D-001206-14-05), siGENOME Mouse Hcar2 siRNA (si*Hcar2*; M-040890-00-0005), and siGENOME Mouse Hnrnpa1 siRNA (si*Hnrnpa1*; M-040887-01-0005), were purchased from Horizon Discovery. The oligos were transfected into mouse primary microglia using INTERFERin (101000028; Polyplus), following the manufacturer's protocol. Cells were transfected 24 hours before other experimental interventions, such as the application of LPS.

qPCR

RNA was isolated by Quick-RNA MicroPrep Kit (R1051; Zymo Research), cDNA synthesis was carried out with Superscript cDNA Synthesis Kit (1708891; BioRad), and qPCR was performed using iTaq Universal SYBR Green Supermix (1725121; BioRad) in a BioRad CFX96 Real-Time System. Gene expression analyses were normalized to the *B2m* housekeeping gene. The following primers were used: *B2m*: Fw_ACAGTTCCACCCGCCTCACATT, Rv_TAGAAAGACCAGTCCTTGCTGAAG; *Il1b*: Fw_TGGACCTTCCAGGATGAGGACA, Rv_GTTCATCTCGGAGCCTGTAGTG; *Il6*: Fw_TACCACTTCACAAGTCGGAGGC, Rv_CTGCAAGTGCATCATCGTTGTTC; *Ccl2*: Fw_GCTACAAGAGGATCACCAGCAG, Rv_GTCTGGACCCATTCCTTCTTGG; *Hcar2*: Fw_CTGTTTCCACCTCAAGTCCTGG, Rv_CATAGTTGTCCGTCAGGAACGG; *Hnrnpa1*: Fw_CGAAACAACCGACGAGAGTCTG, Rv_CATGGCAGCATCCACTTCTTCC; *Cdkn1a*: Fw_TTGTCGCTGTCTTGCACTCT, Rv_TCTCTTGCAGAAGACCAATC.

Western blotting

Cells and tissues were lyzed by a RIPA buffer (1% NP-40, 1% sodium deoxycholate, 0.1% SDS, 150 mM NaCl, and 25 mM Tris-HCl, pH 7.6) with protease inhibitor cocktail (11836170001; Roche).

For the IL-1β secretion inflammasome assay, proteins in the supernatant were precipitated by chloroform and methanol. These lysates were prepared in sample buffer (NP0007; Invitrogen) with 10% 2-Mercaptoethanol (M6250; Sigma) and loaded onto 4%–20% precast polyacrylamide gels (4561096 or 5671095; Bio-Rad). Imaging was performed with SuperSignal West Femto Maximum Sensitivity Substrate (34096; Thermo Scientific) on an Azure Biosystems c600 imager.

The following antibodies were used: anti-H3K9bhb: PTM-1250, PTM Biolabs; anti-H3K9ac: #9496, Cell Signaling; anti-H3: 07-690, Millipore; anti-Gapdh: 60004-1-lg, Proteintech; anti-HSP90: 610419, BD Biosciences; anti-Kac: #9441, Cell Signaling; anti-Kbhb: PTM-1201, PTM-Biolabs; anti-IL-1β: GTX74034, GeneTex; anti-mouse IgG: #7076, Cell Signaling; anti-rabbit IgG: #7074, Cell Signaling. The bands were quantified using Fiji software (https://fiji.sc).

IL-1β enzyme-linked immunosorbent assay (ELISA)

IL-1β secretion was detected using an IL-1 beta Mouse Uncoated ELISA Kit (88-7013-88; Invitrogen), following the manufacturer's protocol.

Quantification and statistical analysis

Figures are presented as mean ± standard deviation, and p-values are calculated by unpaired two-tailed t-test with the assumption of Gaussian distributions or one-way ANOVA with additional post hoc testing for group comparisons. In the figures, p-values are denoted by real values or asterisks (*$p < 0.05$, **$p < 0.01$, ***$p < 0.001$, ****$p < 0.0001$). Correlations are calculated using Pearson correlation or simple linear regression. Statistical analyses were conducted using GraphPad Prism 10 (GraphPad Software). In **Supplemental Figure 2B**, one value was identified as an outlier by both the ROUT and Grubb's tests and removed.

Results

Fourteen-month Cyclic KD reduces age-induced neuroinflammation

In a previous study, we demonstrated that C57BL/6JN male mice started on alternate-week Cyclic KD at 12 months old exhibited enhanced survival and healthspan, particularly memory function[15]. During the KD-fed weeks, peak plasma levels of R-BHB in Cyclic KD-fed mice were 1.5–2.5 mM[15], and we later found that one-week KD increases brain R-BHB levels more than 10-fold[51]. The mechanism by which exposure to KD and ketone bodies, including R-BHB, affected memory and aging phenotypes was not known. We hypothesized that long-term Cyclic KD may mitigate age-induced chronic neuroinflammation, based on several known mechanisms by which BHB regulates inflammation[4,9,52] and recent studies showing that short-term or alternating KD has a more favorable effect on inflammation than long-term continuous KD. Goldberg *et al.* found that four-month continuous *ad libitum* KD promotes obesity and adipose chronic inflammation in mice, while one-week KD activates γδ T cells in adipose tissue and restricts inflammation[14]. Wei *et al.* showed that continuous KD induces cellular senescence in multiple organs, including the brain and liver, while intermittent KD (alternating four-day KD and seven-day CD for three cycles) was observed to not induce senescence[11]. To explore the impact on transcriptional expression in the brain of one-week KD for 12-month-old mice and 14-month Cyclic KD for 26-month-old mice (12-month-old mice maintained on Cyclic KD for 14 months), we carried out bulk RNA-Seq followed by GSEA on whole brain samples from our published cohorts[15] (**Fig. 1A**). The tissue samples had been collected during a CD feeding period in order to best identify persistent long-term effects related to aging rather than transient acute effects of KD. We found that one-week KD, aging from 12 to 26 months (CD), and 14-month Cyclic KD each altered the expression of numerous genes (**Supplemental Fig. 1A–C**). One-week KD induces several MSigDB hallmark pathways such as "Hedgehog Signaling," "Notch Signaling," and "Inflammatory Signaling" in the brain (**Supplemental Fig. 1D** and **Supplemental Table 1**). We observed an induction of genes related to ketone metabolism during one-week KD (**Supplemental Fig. 2B**). However, lysine acetylation (Kac) and Kbhb

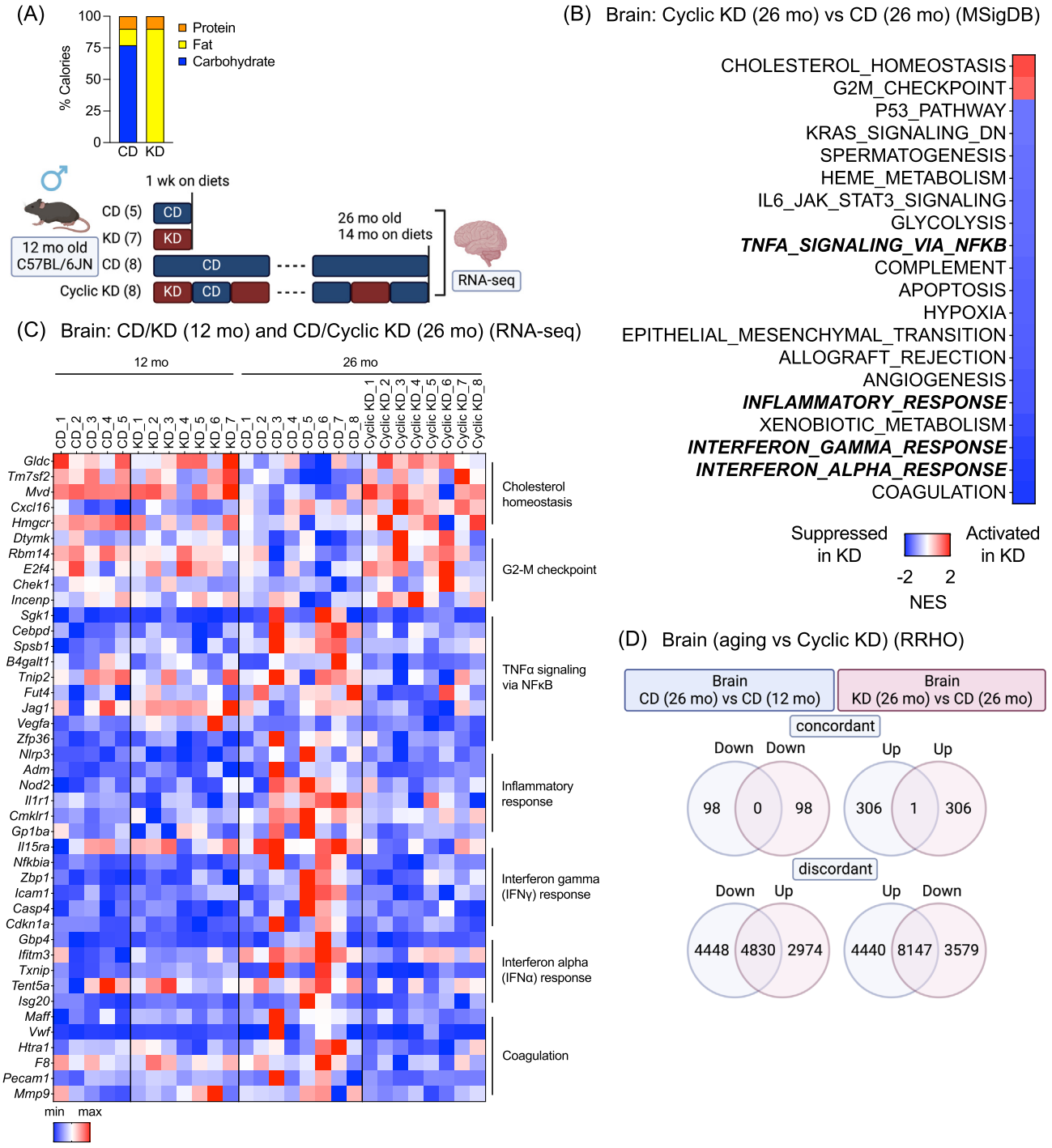

Figure 1. Fourteen-month Cyclic ketogenic diet (Cyclic KD) reduces age-induced neuroinflammation. (**A**) Diet composition and experimental timeline. Brains were harvested at 12 months old (12-month-old mice maintained on control diet [CD] [CD (12 months), n = 5] or KD [KD (12 months), n = 7] for one week) and at 26 months old (12-month-old mice maintained on CD [CD (26 months), n = 8] or Cyclic KD [Cyclic KD (26 months), n = 8] for 14 months), collected at a dark cycle during a CD-fed week. (**B**) Gene set enrichment analysis (GSEA) (Molecular Signatures Database [MSigDB]) in the brain (Cyclic KD [26 months] vs. CD [26 months]). (**C**) Heatmap of gene expressions in the brain. (**D**) Rank–Rank Hypergeometric Overlap analysis comparing aging (CD [26 months] vs. CD [12 months]) with Cyclic KD (Cyclic KD [26 months] vs. CD [26 months]) in the brain. Abbreviation: NES, normalized enrich score.

were not detected in the brain via Western blot after one-week KD (**Supplemental Fig. 1E**). The brains of 26-month-old CD-fed mice exhibited age-induced chronic inflammatory gene expression profiles compared to 12-month-old CD-fed mice (**Supplemental Fig. 2A,B** and **Supplemental Table 1**). However, 26-month-old mice fed Cyclic KD for 14 months showed decreased expression of inflammation-related pathways induced by aging compared to 26-month-old CD-fed mice, such as "TNFα Signaling via NFκB," "Inflammatory Response," and "Interferon Gamma Response," in the brain (Fig. 1B,C and **Supplemental**

Table 1). Other pathways show similar divergent results between short-term and long-term KD exposure. A GO analysis shows that one-week KD in 12-month-old mice activates angiogenesis-related functions ("angiogenesis," "blood vessel morphogenesis"), which are instead inhibited by 14-month Cyclic KD in 26-month-old mice compared to 26-month-old CD-fed mice (**Supplemental Fig. 3A–C**). A KEGG analysis also found age-induced inflammatory patterns suppressed by long-term KD, specifically "Coronavirus disease—COVID-19" (**Supplemental Fig. 3D–F**). The initial cohorts involved short-term (one week) and long-term (14 months) KD treatment, all starting at 12 months of age. In order to better characterize the effect of short-term KD on aging phenotypes in older mice, we treated a new cohort of 22-month-old mice with one week of KD followed by analysis of selected genes via qPCR (**Supplemental Fig. 2C**). At 22 months of age, one-week KD appears to reduce the expression of several age-induced inflammatory genes, including *Nlrp3*, *Icam1*, and *Mmp9* (**Supplemental Fig. 2C**). Thus, while short-term KD may increase expression of certain inflammatory pathways in younger mice (**Supplemental Fig. 1D**), its effects may diverge by age and reduce certain age-related chronic inflammatory changes in older mice. We employed an RRHO analysis to identify overlapping genes that were altered in the same or opposite direction across paired datasets[44]. In the brain, aging (26-month-old CD vs. 12-month-old CD) and 14-month Cyclic KD (26-month-old KD vs. 26-month-old CD) exhibit gene expression patterns that are almost entirely discordant (**Fig. 1D**), suggesting that 14-month Cyclic KD may partially counteract aging-induced gene expression changes in the brain.

These bulk RNA-Seq datasets were derived from whole brains, which precludes the direct demonstration of cell-type-specific gene expressions. A deconvolution method (CIBERSORTx)[45] was employed to estimate the relative contributions of each cell type in each sample's expression dataset (**Supplemental Fig. 4A**). The algorithm predicted that approximately 70% of detected gene expression originated from neurons, with approximately 15%–20% from astrocytes and the remainder largely from oligodendrocytes (**Supplemental Fig. 4A**). This suggests that the bulk RNA-Seq datasets largely reflect the transcriptional profile of neurons, as expected. We previously reported that the 14-month Cyclic KD regimen suppresses TOR activity and activates a PPARα-driven gene expression pattern in the liver via qPCR analysis[15]. To more systematically examine the changes in liver transcription that occur after 14-month Cyclic KD treatment, we conducted bulk RNA-Seq of liver samples from 12-month-old mice fed CD or KD for one week as well as 26-month-old mice fed CD or Cyclic KD for 14 months (**Supplemental Fig. 5A–C**). We found a significant number of 14-month Cyclic KD-regulated genes (**Supplemental Fig. 5B**). On GSEA analysis, 14-month Cyclic KD suppressed "mTORC1 signaling" and "PI3K AKT mTOR signaling," consistent with the prior qPCR data (**Supplemental Fig. 5C**). 14-month Cyclic KD also led to the suppression of several MSigDB hallmark pathways, including "TNFα Signaling via NFκB," "Interferon Alpha Response," "Inflammatory Response," and "Interferon Gamma Response," which are generally related to chronic inflammation (**Supplemental Fig. 5C,D** and **Supplemental Table 1**). GO and KEGG analyses also revealed that 14-month Cyclic KD suppresses immune response-related pathways such as the "immune system process" (GO) and "Phagosome" (KEGG) (**Supplemental Fig. 6A,B**). One-week KD at 12 months old increased ketone metabolism gene expression but did not obviously alter inflammatory pathways (via reanalysis of a dataset reported previously[15]) (**Supplemental Fig. 6C**).

We noted that hyperinflammatory gene expression patterns in both liver and brain of 26-month-old mice were concentrated in specific animals, all in the CD-fed group (**Fig. 1C** and **Supplemental Fig. 5D**). We investigated the source of this heterogeneity by examining organ weights that were recorded at necropsy. Statistically, 14-month Cyclic KD does not result in a reduction in liver weight compared to the 14-month CD-fed group ($p = 0.07$) (**Supplemental Fig. 7A**). However, four of the 14-month CD-fed mice (CD_3, CD_5, CD_6, and CD_7) had liver weights notably heavier than all other animals in either the CD or KD groups (**Supplemental Fig. 7A**). The four mice with markedly enlarged livers all demonstrated elevated levels of inflammatory signaling (**Supplemental Fig. 5D**). In CD-fed mice, thousands of genes in the liver exhibited either positive or negative correlations with liver weight (**Supplemental Fig. 7B**). In contrast, the number of genes exhibiting such correlations was considerably smaller in 14-month Cyclic KD-fed mice, which had much less variation in liver weight (**Supplemental Fig. 7B**). A pathway analysis conducted using MSigDB revealed a robust positive correlation between liver weight and inflammatory-related gene expression in the livers of mice fed both CD and Cyclic KD. In CD-fed mice, genes associated with fatty acid metabolism and oxidative phosphorylation MSigDB pathways are negatively correlated with liver weight (**Supplemental Fig. 7C**). When we examined specific genes of interest, we observed positive correlations between inflammatory genes (*Cd38*, *Nlrp3*, *Txnip*, and *Icam1*) and liver weight and between cellular senescence genes (*Trp53*, *Cdkn1a*, *H2ax*, *Glb1*, and *Serpine1*) and liver weight (**Supplemental Fig. 7D**). In contrast, a negative correlation was observed between the expression of ketogenic genes (*Cpt1a*, *Acat1*, *Hmgcs2*, *Hmgcl*, and *Bdh1*) and liver weight (**Supplemental Fig. 7D**). These findings suggest that hepatomegaly associated with chronic inflammatory gene expression was common among aged CD-fed mice, but this phenotype appeared to be ameliorated by long-term Cyclic KD, despite the intermittent exposure of these mice to the very high-fat KD.

Our RRHO analysis showed that 14-month Cyclic KD generating highly concordant expression patterns across tissues (brain and liver), although they do not overlap completely (**Supplemental Fig. 8A**). Furthermore, we identified a number of genes whose expression levels exhibited a positive correlation between the liver and the brain (**Supplemental Fig. 8B**). MSigDB pathway analysis showed that inflammation-related pathways are highly involved in the observed positive correlations, especially in aged CD-fed mice (**Supplemental Fig. 8C**). For instance, expression levels of both inflammatory genes (*Txnip*, *Gbp4*, *Nfkbia*, and *Icam1*) and genes involved in cellular senescence (*Cdkn1a* and *Serpine1*) both show high degrees of correlation between liver and brain of 26-month-old mice fed CD for 14 months (**Supplemental Fig. 8D**). These correlations were attenuated or absent in 26-month-old mice fed Cyclic KD for 14 months and in 12-month-old mice fed either CD or KD for one week (**Supplemental Fig. 8D,E**). Interestingly, we observed strong correlations between liver weight and brain gene expression in aged mice, including inflammatory-related pathways and cellular senescence genes, particularly in the CD-fed group (**Supplemental Fig. 9A–C**). These findings indicate that excessive liver weight was associated with not only chronic inflammation and cellular senescence in the liver, as expected, but also in the brain. Long-term Cyclic KD may have the potential to

interrupt such inter-organ effects of aging. Recent studies suggest that KD and BHB can improve T cell function in both humans and mice[53–55]. To examine the impact of Cyclic KD on age-related changes to immune cell subsets, blood samples were collected and analyzed from a different subset of mice in the previously published cohorts[15] at 24 months of age after 12 months of Cyclic KD or CD feeding (**Supplemental Fig. 10A**). As with the cohort that contributed brain and liver specimens, these samples were collected during a CD feeding period. Additional groups of strain-matched 3-month-old and 12-month-old mice provided younger age norms. As expected, $CD8^+$ cells increased as a proportion of all T cells with age, while $CD4^+$ cells decreased. Cyclic KD did not significantly alter the individual proportions of either $CD4^+$ or $CD8^+$ cells; however, it significantly reversed the $CD8^+/CD4^+$ ratio that is a hallmark of pro-inflammatory immune aging[56] (**Supplemental Fig. 10B**). Cyclic KD did not alter the populations of key regulatory subsets, including $Foxp3^+/CD4^+$, PD-$1^+/CD4^+$, and PD-$1^+/CD8^+$ T cells (**Supplemental Fig. 10C,D**). Direct or indirect modulation of age-related immune inflammation could be a mechanism by which Cyclic KD alters inter-organ inflammatory effects.

R-BHB reduces LPS-induced inflammation in human primary microglia

We next focused on mechanisms of directly regulating brain inflammation. In mice, one-week KD induces hepatic R-BHB production and increases plasma and brain levels by more than tenfold[51]. We hypothesize that R-BHB can directly modulate acute and chronic neuroinflammation. To examine the transcriptional effects of R-BHB on brain cells, we employed *in vitro* culture models for human primary microglia, astrocytes, and neurons. Chronic inflammation is a hallmark of both brain aging and neurodegenerative diseases[57,58]. There are no established *in vitro* systems that precisely model age-induced chronic inflammation, but to simulate inflammation *in vitro*, we used LPS, which is widely used to induce acute brain inflammation in *in vivo* models, including in aging[59]. As individuals age, the microglia, which are the immune cells of the brain, become more active and induce the production of pro-inflammatory cytokines[60]. Our preliminary experiment varying the exposure time to LPS demonstrated that a six-hour LPS incubation most strongly induces inflammatory cytokine production in human primary microglia (**Supplemental Fig. 11A**). We then incubated cells for 24 hours with 10 mM R-BHB (acid), the endogenous form of BHB induced by ketosis, adding LPS during the final six hours. Gene expression was analyzed by RNA-Seq (**Fig. 2A**). Volcano plots show that 10 mM R-BHB substantially altered gene expression in all three cell types, both with and without LPS stimulation (**Supplemental Fig. 11B–D**). LPS had the most pronounced effect on microglial gene expression, with only a modest impact on astrocytes and even less on neurons (**Supplemental Fig. 11B–D**). MSigDB analysis indicates that in the absence of LPS stimulation, R-BHB upregulates inflammatory signaling through "TNFα Signaling via NFκB" and "Inflammatory Response," while inhibiting cell cycle regulation pathways via "Mitotic Spindle" and "G2-M Checkpoint" in all three types of cells (**Fig. 2B**, **Supplemental Fig. 12B–D**, and **Supplemental Table 2**). LPS stimulation markedly activates a wide range of inflammatory signaling pathways in microglia, and, to a lesser extent, in astrocytes but not in neurons (**Supplemental Fig. 12A** and **Supplemental Table 2**). Combined with LPS stimulation, R-BHB treatment resulted in the further activation of a limited number of inflammatory-related genes (such as *HIF1A* and *CDKN1A*) in all three cell types (**Supplemental Fig. 12C,D**). However, the dominant effect in microglia was a profound overall reduction in expression of other inflammation-related genes and pathways, including "TNFα Signaling via NFκB," "Inflammatory Response," "Interferon Alpha Response," and "Interferon Gamma Response" (**Fig. 2C**, **Supplemental Fig. 12C–E**, and **Supplemental Table 2**). In microglia, LPS stimulation also reduced the expression of genes involved in ketogenesis, specifically *CPT1A*, *HMGCL*, and *BDH1*. R-BHB induced certain monocarboxylate transporters (MCTs) in a cell-dependent manner. For instance, *SLC16A7* expression was increased in neurons, and *SLC16A6*, *SLC16A10*, and *SLC16A14* were increased in microglia (**Supplemental Fig. 12F**), which suggests cell-specific regulation of ketone transport in the brain. GO and KEGG analyses generated concordant results, with R-BHB suppressing LPS stimulation of several inflammatory pathways in microglia but not neurons and astrocytes, including the "innate immune response" (GO) and "Chemokine signaling pathway" (KEGG) (**Supplemental Figs. 13A–C** and **14A–C**). In summary, R-BHB modifies the brain transcriptome in a cell-specific manner, potentially inducing inflammation in astrocytes and neurons while exhibiting anti-inflammatory effects on microglia, especially in the context of inflammatory stimulation by LPS.

To test the relevance of this *in vitro* model, we next carried out a comparison between the *in vivo* mouse brain datasets (**Fig. 1**) and *in vitro* human primary cell datasets (**Fig. 2**). Comparing the effect of one-week KD in 12-month-old mice (*in vivo*) versus R-BHB on cells (*in vitro*, without LPS) generates discordant patterns for astrocytes and neurons but a concordant pattern for microglia (**Supplemental Fig. 15A**). There is little concordance or discordance between mice aging 12 to 26 months old on CD (*in vivo*) and LPS (*in vitro*) across any of the three cell types (**Supplemental Fig. 15B**). However, the effects of 14-month Cyclic KD on the brains of aged mice (*in vivo)* and of the combination of R-BHB with LPS (*in vitro*) yield concordant gene expression signatures in microglia (but not astrocytes or neurons), similar to what we observed above between one-week KD in younger mice and R-BHB in microglia (**Supplemental Fig. 15C**). Our deconvolution analysis indicated that most of the gene expression captured by RNA-Seq in the brain originates from neurons and not microglia (**Supplemental Fig. 4A**). Nevertheless, these findings indicate that microglial gene expression changes identified *in vitro* are more closely aligned with overall *in vivo* brain expression changes caused by BHB, whether in alone or in the context of age/LPS-related inflammation, than changes induced in astrocytes or neurons.

BHB acids reduce LPS-induced inflammation in mouse primary microglia

Next, in order to establish a system for carrying out more systematic mechanistic experiments than possible with human pri mary cells, we investigated the dose-dependent anti-inflammatory effects of R-BHB in mouse primary microglia. We followed the same time course as described in the *in vitro* RNA-seq study in **Figure 2A** (**Fig. 3A**). R-BHB at both 5 and 10 mM effectively suppressed LPS-induced inflammatory cytokine expression from primary mouse microglia, including IL-1β (*Il1b*), IL-6 (*Il6*), and TNFα (*Tnf*), whereas the chemokine (C-C motif) ligand 2 (*Ccl2*) remained unaffected. At 1 mM concentration, R-BHB had no effect (**Supplemental Fig. 16B**). Altering the timing of exposure to R-BHB showed that R-BHB can inhibit LPS-induced inflammatory activation either when added simultaneously with

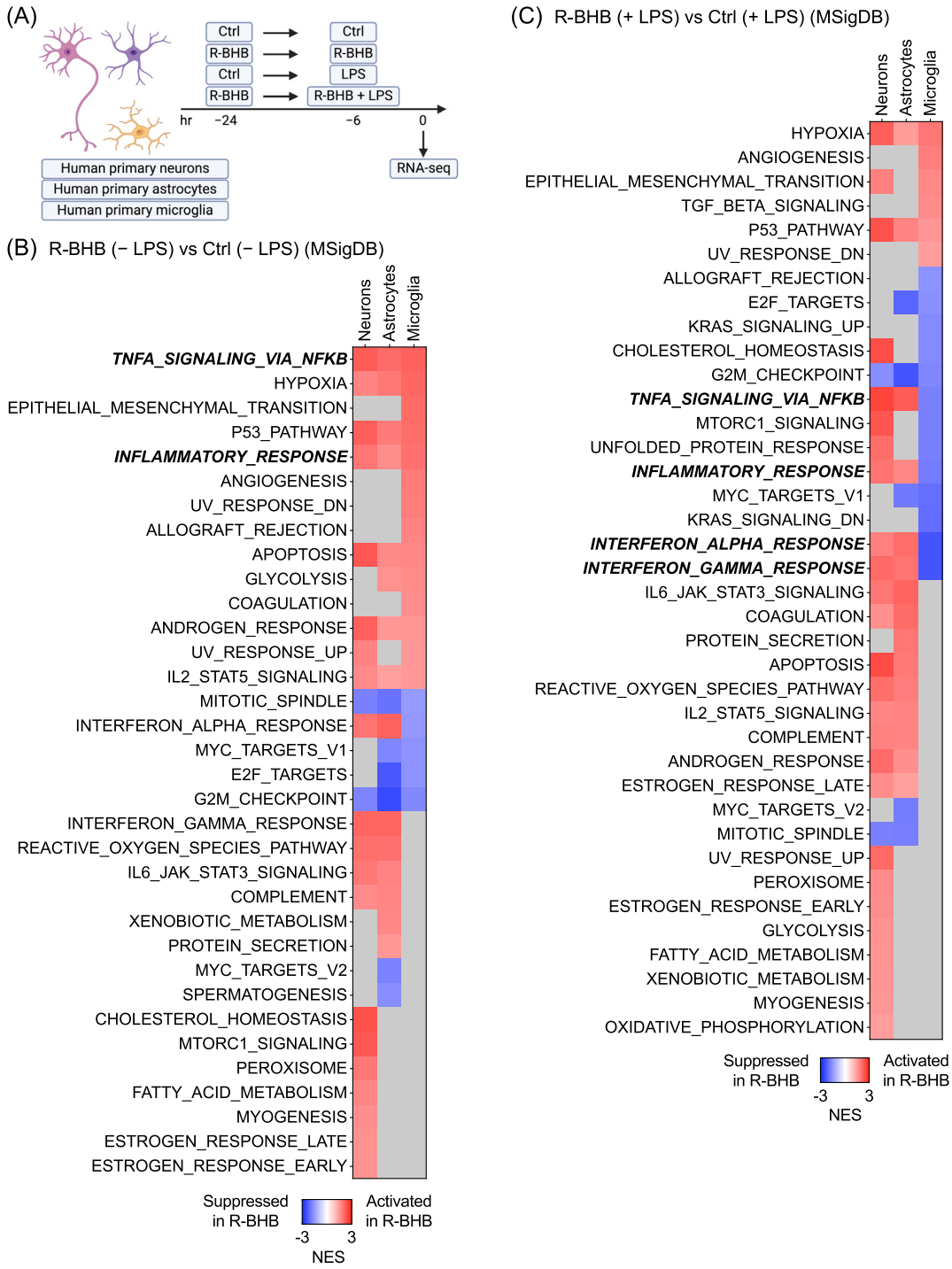

Figure 2. R-beta-hydroxybutyrate (R-BHB) reduces lipopolysaccharide (LPS)-induced inflammation in human primary microglia. (**A**) Experimental timeline. (**B,C**) GSEA (MSigDB) analysis (R-BHB vs. Ctrl) (**B**) without or (**C**) with LPS treatment in human primary neurons, astrocytes, and microglia (n = 3 per group). Gray squares: not significant.

LPS without any preincubation period or when preincubated and removed prior to adding LPS (**Supplemental Fig. 16C,D**), suggesting that the anti-inflammatory effects of R-BHB are both acute and prolonged for several hours in this *in vitro* culture model.

Published literature suggests a variety of possible mechanisms by which R-BHB may regulate inflammation in microglia, such as energy supply[61], HDAC inhibition[62], regulation of Kbhb[7], NLRP3 inflammasome inhibition[4,63], HCAR2 activation[52,64], and interaction with hnRNP A1[9]. To test these mechanisms, we used both free acid and sodium salt forms of both BHB enantiomers (R-BHB, S-BHB, Na-R-BHB, and Na-S-BHB), each at a concentration of 10 mM. We also tested the structurally related non-ketone body short-chain fatty acid butyrate, which is a more potent HDAC inhibitor[65], in both free acid (Bu) and sodium salt (Na-Bu) forms at a concentration of 5 mM (**Supplemental Fig. 16A**). The addition of R-BHB, S-BHB, or butyrate-free acids at or above 5 mM to

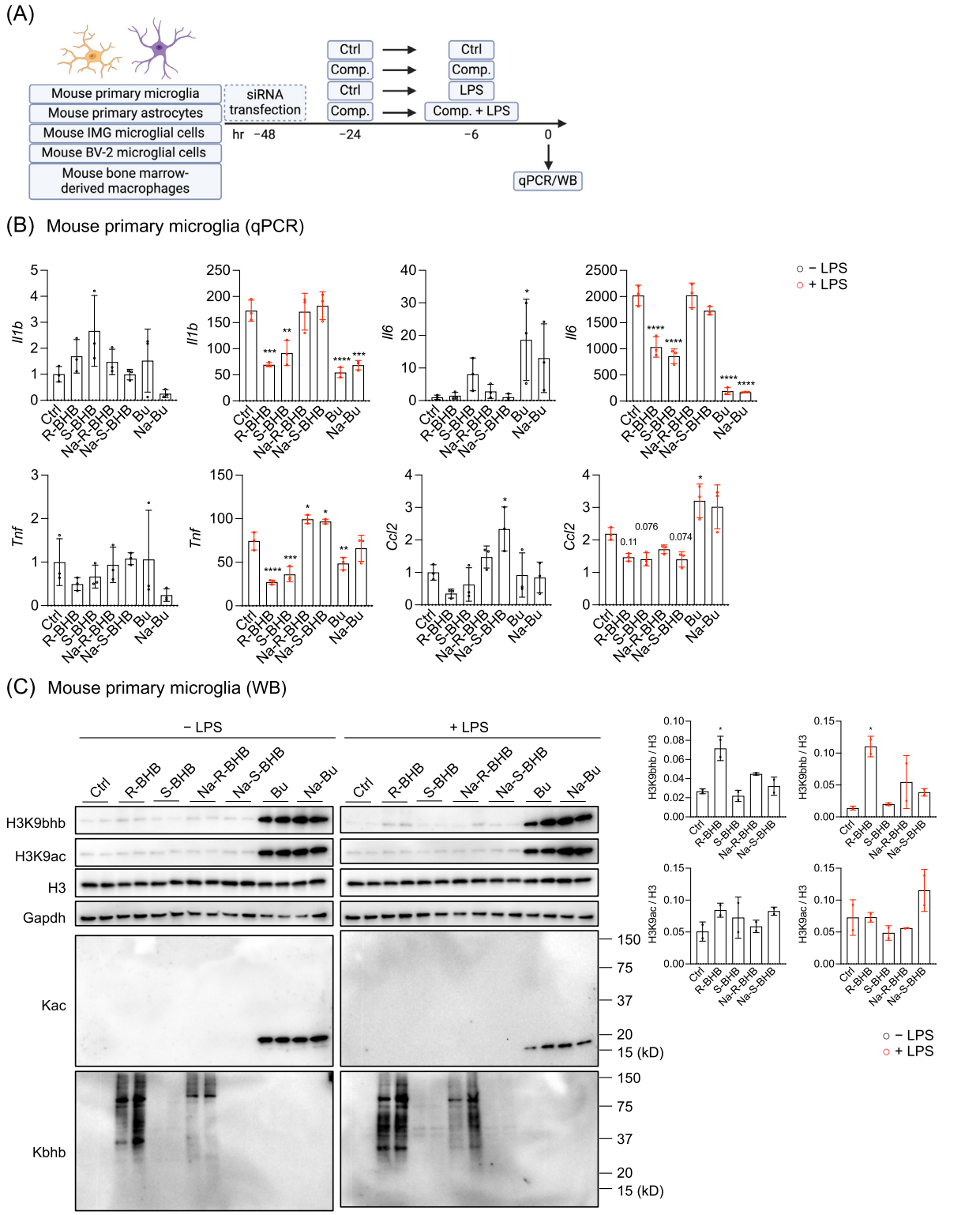

Figure 3. BHB acids reduce LPS-induced inflammation in mouse primary microglia. (**A**) Experimental timeline. (**B**) mRNA expression in mouse primary microglia (n = 3 per group). All data are presented as mean ± standard deviation (SD). One-way ANOVA with Dunnet's correction for multiple comparisons. Compare the mean of each sample with the mean of "Ctrl." (**C**) Protein expression and the quantification in mouse primary microglia (n = 2 per group). All data are representative of two independent experiments. Compare the mean of each sample with the mean of "Ctrl." Abbreviations: R-BHB, R-BHB acid; S-BHB, S-BHB acid; Na-R-BHB, R-BHB sodium salt; Na-S-BHB, S-BHB sodium salt; Bu, butyric acid; and Na-Bu, butyrate sodium salt.

the buffered culture medium resulted in a slight reduction in pH (**Supplemental Fig. 16A**). In contrast, the addition of the sodium salts did not result in a change in pH (see **Supplemental Fig. 16A**). A Seahorse assay was employed to ascertain whether R-BHB or S-BHB increases oxygen consumption rate (OCR) in mouse primary microglia as a proxy for oxidative metabolism

(**Supplemental Fig. 16E**). OCR was higher in cells treated with R-BHB than S-BHB, though the increase with R-BHB over control did not reach statistical significance (**Supplemental Fig. 16E**). These data suggest that R-BHB but not S-BHB can be modestly metabolized as an energy source by microglia over a period of minutes, as expected given that S-BHB cannot be metabolized by the enzyme BDH1 in the canonical ketone body oxidation pathway[66] and is oxidized only incompletely via alternative indirect metabolic pathways[67]. The administration of R-BHB, S-BHB, Bu, and Na-Bu, but not Na-R-BHB and Na-S-BHB, resulted in a reduction in the expression of inflammatory cytokines in the presence of LPS (**Fig. 3B**). Therefore, BHB chirality and energy metabolism of R- versus S-BHB do not appear to determine the anti-inflammatory effect observed in microglia, and the effect is shared by butyrate.

Since both R-BHB and butyrate function as HDAC inhibitors[6,65], and HDACs regulate transcriptional activation, we hypothesized that HDAC inhibition might be the underlying mechanism inhibiting inflammatory gene activation in microglia. R-BHB also regulates Kbhb posttranslational modification, which may also have a role in regulating transcriptional activation[7]. We therefore assessed protein lysine acetylation (Kac) and Kbhb by western blotting to analyze how these compounds affect epigenetic modifications in microglia (**Fig. 3C**). Without LPS, R-BHB and Na-R-BHB both significantly increased protein Kbhb (the antibody is R-enantiomer-specific).

Additionally, both compounds showed a mild increase in histone 3 lysine 9 beta-hydroxybutyration (H3K9bhb) while not affecting Kac or histone 3 lysine 9 acetylation (H3K9ac). On the other hand, both Bu and Na-Bu substantially increased the levels of H3K9bhb, H3K9ac, and Kac but not global Kbhb. These effects were all similar in the presence of LPS (**Fig. 3C**). As we did not observe Kac or H3K9ac changes with R-BHB (but did with Bu and Na-Bu), HDAC inhibition appears unnecessary for the microglial anti-inflammatory effect. We then investigated other reported mechanisms by which BHB regulates inflammation in various cell types. BHB activates HCAR2, which has been reported to be necessary for BHB's neuroprotective effect[52,64]. BHB also directly binds to hnRNP A1 and upregulates *Oct4*, a regulator of quiescence and senescence, in both vascular smooth muscle and endothelial cells[9]. We utilized siRNAs targeting HCAR2 (*Hcar2*) and hnRNP A1 (*Hnrnpa1*) to examine the respective functions of these genes in primary mouse microglia (**Supplemental Fig. 17A**). Both siRNAs decreased gene expression by approximately 50%. LPS-induced *Hcar2* expression 100-fold over baseline but did not affect *Hnrnpa1* expression. Knockdown of either *Hcar2* or *Hnrnpa1* did not affect R-BHB suppression of inflammatory gene expression after LPS (**Supplemental Fig. 17A**), indicating that BHB's anti-inflammatory effects in mouse primary microglia are independent of HCAR2 activation or hnRNP A1 binding. Next, we investigated NLRP3 inflammasome activation, which is inhibited by BHB in mouse primary macrophages[4], in our mouse primary microglia model (**Supplemental Fig. 18A**). We used MCC950, a pharmacological NLRP3 inflammasome inhibitor, as a positive control. All BHB compounds had no effect on IL-1β secretion after ATP-induced NLRP3 inflammasome activation (**Supplemental Fig. 18B,C**). In fact, the acid forms of R- and S-BHB, along with Bu and Na-Bu, actually increased nigericin-induced NLRP3 inflammasome activation (**Supplemental Fig. 18B,C**). Therefore, modulation of NLRP3 inflammasome activation by BHB appears to be specific to the cell type and the activation signals involved, and NLRP3 inflammasome inhibition does not explain the microglia anti-inflammatory effect.

Recently, KDs were found to promote cellular senescence, though brief alternating periods of KD (similar to our Cyclic KD) prevented senescence[11]. The aspect of KD responsible for these effects was not identified, although prior work showed that BHB can prevent vascular senescence[9]. We sought to test if BHB might reduce chronic neuroinflammation *in vivo* via reducing senescence in the brain, using mouse primary microglia with three different cellular senescence inducers: IR, H_2O_2, and AA. Recent studies suggest IR accelerates cellular brain aging, including in microglia[68]. BHB has been reported to prevent H_2O_2-induced cellular senescence in human umbilical vein endothelial cells[9] and AA-induced cellular senescence in NIH-3T3 fibroblast cells[11]. In primary microglia, all three senescence inducers were capable of increasing *Cdkn1a* expression, a key gene associated with cellular senescence[69] (**Supplemental Fig. 19A–C**). BHB reduced *Cdkn1a* expression in IR- or H_2O_2-stimulated microglia (**Supplemental Fig. 19A,B**), consistent with a role in reducing senescent transformation. Other inflammatory genes, such as those induced by LPS (*Il1b*, *Il6*, *Tnf*), were not generally increased upon senescence induction. Prevention of senescence in the brain could be a mechanism by which BHB modulates chronic age-related neuroinflammation, though this will depend on the extent to which neuroinflammation is driven by senescent cells. We further investigated the cell-specific effects of different forms of BHB in mouse primary astrocytes (**Supplemental Fig. 20A,B**), two microglia cell lines (IMG[70] [**Supplemental Fig. 21A–C**] and BV-2[71] cells [**Supplemental Fig. 22A–C**]), and BMDMs (**Supplemental Fig. 23A–C**). In primary astrocytes, R-BHB and S-BHB free acids demonstrated a reduction solely in *Tnf* expression (**Supplemental Fig. 20A**), while the effects of various BHB forms on Kac and Kbhb expression patterns were similar to those observed in primary microglia (**Supplemental Fig. 20B**). In IMG cells, R-BHB and S-BHB free acids modestly potentiated LPS-induced inflammation (**Supplemental Fig. 21A**) and also potentiated activation of the NLRP3 inflammasome with both ATP and nigericin (**Supplemental Fig. 21B**). All forms of BHB increased the levels of both H3K9bhb and H3K9ac (**Supplemental Fig. 21C**). In BV-2 cells, all forms of BHB had little impact on either LPS-induced inflammation or NLRP3 inflammasome activation (**Supplemental Fig. 22A,B**). All forms of BHB-induced H3K9bhb, but not H3K9ac (**Supplemental Fig. 22C**). In BMDMs, the acid forms of BHB reduced inflammatory gene expression (**Supplemental Fig. 23A**) but potentiated nigericin-induced activation of the NLRP3 inflammasome (**Supplemental Fig. 23B**). Both acid and salt forms of R-BHB-induced H3K9bhb levels but not H3K9ac in BMDMs (**Supplemental Fig. 23C**). In summary, these results indicate that BHB acids consistently decrease LPS-induced inflammatory gene expression in primary microglia but that the effects on inflammation and inflammatory mechanisms vary in other brain cell types as well as other innate immune cell types.

BHB acids reduce LPS-induced inflammation potentially through minor pH fluctuations

Not yet having identified a specific mechanism for microglia inflammatory modulation, we next turned to the potential biochemical adjuvants of BHB activity. *In vivo*, release of R-BHB into the blood creates an acidosis that, when unregulated, overcomes endogenous buffering to cause an acidemia. Movement of BHB

across cell membranes and through intracellular compartments might similarly alter the acid-base environment locally; the MCTs of BHB are proton-anion cotransporters. Above, we found that *in vitro* only the free acids, but not the sodium salts, of BHB generated an anti-inflammatory effect in primary mouse microglia despite buffering. We therefore tested whether the sodium present in Na-R-BHB or Na-S-BHB and/or the slightly acidic environment resulting from R-BHB or S-BHB incubation might modulate inflammatory signaling. In mouse primary microglia, the addition of 10 mM NaCl does not alter the anti-inflammatory responses by R-BHB (**Supplemental Fig. 24A**), suggesting sodium salt by itself does not affect inflammatory regulation. Next, we modulated the pH in the culture medium using either 6.75 mM NaOH, which reverses the change in medium pH by 10 mM R-BHB, or 15 mM HCl, which reduces the medium pH of 10 mM Na-R-BHB-added medium to a degree comparable to that of 10 mM R-BHB-free acid (**Supplemental Fig. 16A**). The addition of NaOH partially attenuates the anti-inflammatory effect of R-BHB (Fig. 4A). The addition of HCl to Na-R-BHB-supplemented medium, as well as HCl alone, appears sufficient to reduce inflammatory gene expression activation (Fig. 4A). These small pH changes do not affect ATP-induced NLRP3 inflammasome activation (**Supplemental Fig. 24B**). For nigericin-induced NLRP3 inflammasome activation, HCl enhances activation similar to R-BHB, while NaOH strongly inhibits activation and may attenuate the increased activation by R-BHB free acid (Fig. 4B). Altogether, these findings show that the pathways by which BHB regulates inflammation and the NLRP3 inflammasome may be influenced by small pH fluctuations and/or the availability of free anions in the local cellular milieu.

Discussion

Here, we show that 14-month Cyclic KD started at 12 months of age reduced age-induced chronic inflammation in the mouse brain (Fig. 1). R-BHB substantially modifies the transcriptional response to LPS in human and mouse primary microglia, largely reducing inflammatory transcriptional activation while having modest pro-inflammatory effects under basal conditions in microglia, neurons, and astrocytes (Fig. 2). In mechanistic experiments with mouse primary microglia, we found that inhibition of the inflammatory response by the acid forms of R- and S-BHB requires a change in pH or anion availability but does not work through energetic supply or any of the previously known mechanisms of BHB inflammatory modulation (Figs. 3 and 4). Importantly, we found both pro- and anti-inflammatory effects of BHB depending on cell type and context. Overall, R-BHB *in vitro* exerts a modest pro-inflammatory effect in the absence of LPS while exhibiting an overall potent anti-inflammatory impact when microglia are activated by LPS. Similarly, one-week KD feeding in middle-aged (12-month-old) mice generates a modest pro-inflammatory gene expression

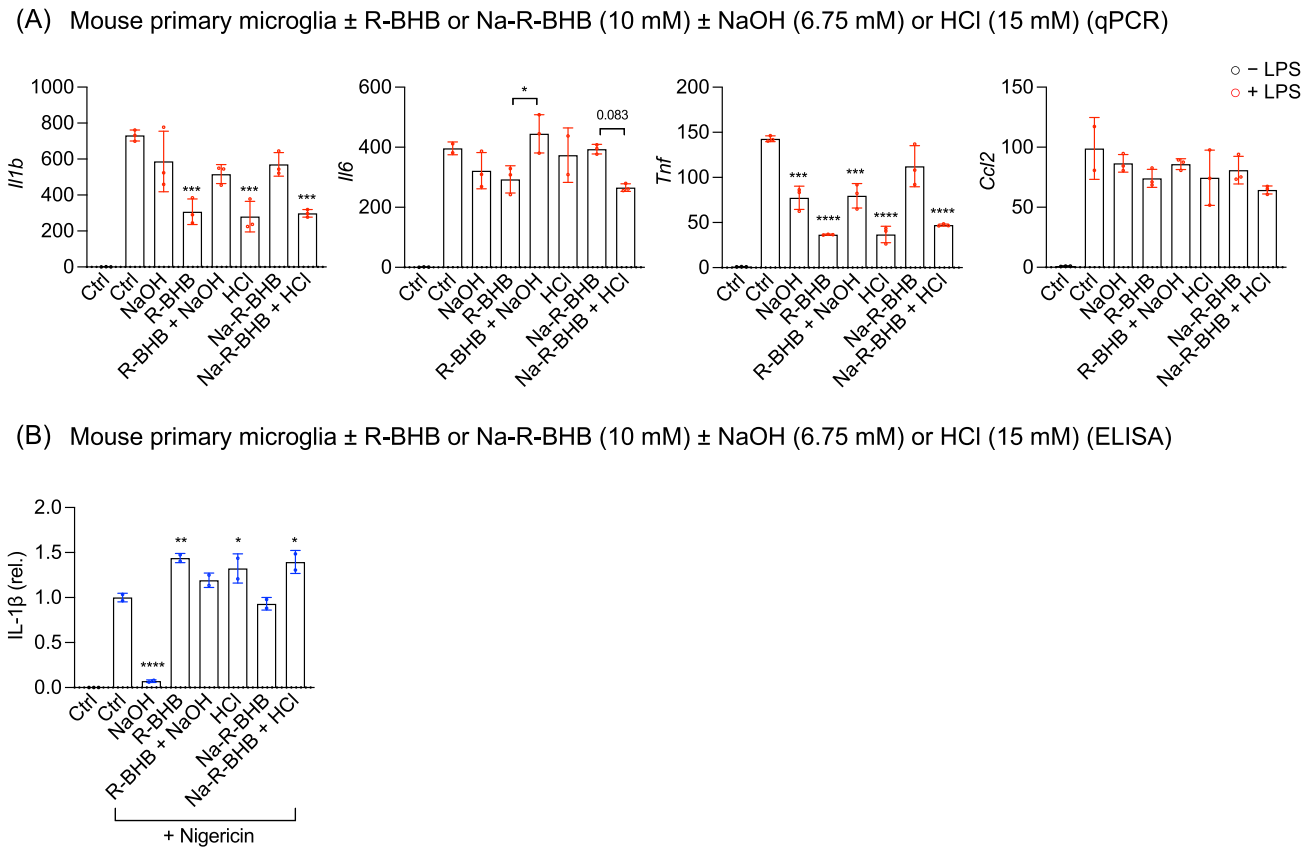

Figure 4. BHB acids reduce LPS-induced inflammation potentially through minor pH fluctuations. (**A**) mRNA expression in mouse primary microglia (n = 3 per group). All data are presented as mean ± SD. One-way ANOVA with Dunnet's correction for multiple comparisons. Compare the mean of each sample with the mean of "Ctrl + LPS." (**B**) IL-1β enzyme-linked immunosorbent assay analysis of IL-1β secretion after NLRP3 inflammasome activation in mouse primary microglia (n = 2 per group). All data are presented as mean ± SD. One-way ANOVA with Dunnet's correction for multiple comparisons. Compare the mean of each sample with the mean of "Ctrl + nigericin." All data are representative of two independent experiments.

signature compared to age-matched controls, while both one-week KD (at 26 months old) and long-term Cyclic KD (from 12 to 26 months old) suppress inflammatory gene expression in the pro-inflammatory context of aging. Continuous versus intermittent KD in mice also have distinct effects on obesity, metabolic maladaptation, and cellular senescence[11,14,15]. These context-dependent effects may help explain apparently discrepant results in the literature in human and mouse studies of ketone bodies and global inflammation and suggest careful attention to context in human studies.

We and another group previously showed that long-term feeding of KD while preventing obesity improved both survival and memory function in aging mice[15,20]. There are likely multiple overlying mechanisms, with differing cell specificity contributing to this memory phenotype. BHB has been reported to regulate inflammation via energetics, the NLRP3 inflammasome, histone modifications, and cell surface receptors. We also recently reported that R-BHB activates protein kinase A and stimulates brain-derived neurotrophic factor in neurons, contributing to remodeling the aging cortical synaptic proteome[72]. Using chemical and genetic tools, we carefully tested the role of a number of known BHB mechanisms in the suppression of inflammatory transcriptional activation that we observed *in vitro*.

The primary role of BHB is to provide energy to cells and tissues[2]. Neurons[73,74], $CD4^+$ T cells[53,54], $CD8^+$ T cells[53,55], and microglia[61] (though not macrophages[75]) all oxidize BHB to generate ATP and intermediate metabolites. The (S) enantiomer of BHB is a useful tool for interrogating mechanisms of BHB action, and it is not produced by ketogenesis (endogenously it is a by-product of fatty acid oxidation) and is oxidized indirectly and more slowly than R-BHB[2,66] while retaining most protein-interacting signaling functions of R-BHB. Both enantiomers demonstrated a comparable reduction in inflammatory gene expression (**Fig. 3B**), while our OCR analysis in microglia confirmed that S-BHB is not substantially oxidized within a timeframe relevant to this effect (**Supplemental Fig. 16E**).

BHB is a known inhibitor of class I HDACs[6], and HDAC inhibitors have anti-neuroinflammatory properties[76]. But while we found that the HDAC inhibitor butyrate (in both acid and sodium salt forms) significantly decreased inflammation in mouse primary microglia *in vitro* (**Fig. 3B**), BHB did not induce histone acetylation (H3K9ac and total Kac around 17 kD [molecular weight of histone H3]) in primary microglia (**Fig. 3C**) under conditions in which BHB demonstrated an anti-inflammatory effect. Similarly, the effect of BHB on histone Kbhb across various cell types was inconsistent with its anti-inflammatory effect. Furthermore, the H3K9bhb antibody may nonspecifically recognize non-Kbhb modifications of histones[77], and the presence of Kbhb in the brain is controversial[78–80]. We found no obvious associated changes in brain total protein Kac or Kbhb levels on KD (**Supplemental Fig. 1E**). It is unlikely that these epigenetic effects of BHB control the anti-inflammatory response we observed. We did not observe a consistent relationship across cell types between reduced inflammatory transcription and decrease in NLRP3 inflammasome activation by BHB[4] across cell types, using both ATP and nigericin as secondary inflammasome activators. Instead, our data suggest that BHB regulation of inflammasome activity in the central nervous system may be complex and context-dependent. Acid forms of BHB in fact amplified nigericin-induced NLRP3 inflammasome activation in primary microglia (**Supplemental Fig. 18B,C**). BHB inhibits the NLRP3 inflammasome by preventing potassium (K^+) efflux[4], while in human primary macrophages, an acidic environment stimulates the NLRP3 inflammasome by enhancing K^+ efflux[81]. And while in macrophages BHB inhibits K^+ efflux, the opposite has been reported in endothelial cells as a mechanism of BHB-induced vasodilation[82]. A comprehensive investigation of the mechanisms by which BHB regulates the NLRP3 inflammasome in the brain, specific to activator and cell type, is imperative. BHB is also an endogenous agonist of the GPCR HCAR2, with neuroprotective[52,83] and peripheral anti-inflammatory effects[84,85], and binds directly to hnRNP A1, which stabilizes the mRNA and increases expression of the Yamanaka factor *Oct4*, thereby preventing endothelial cellular senescence. However, knockdown of neither *Hcar2* nor *Hnrnpa1* abrogates the effect of BHB on inflammatory transcription. Altogether, none of the tested known mechanisms of BHB that modulate inflammation were primarily responsible for our observed anti-inflammatory effect.

While our data do not identify the specific binding target of BHB responsible for this anti-inflammatory effect, they do show that an excess of a small anion (BHB anion or chloride anion) and a small pH change (or sufficient anion excess to be reflected in pH) both appear to be required. Physiologically, the endogenous production of ketones induces a metabolic acidosis that is well compensated in blood under normal conditions[86]. However, there may be meaningful changes in pH in specific compartments: KD induces intracerebral acidosis (from pH 7.2 to 6.9), which has anticonvulsant effects in a rat model of infantile spasms[87], and the acid form of BHB inhibits the growth of *Bifidobacterium in vitro* by a pH-dependent mechanism[16]. Furthermore, there are examples of small anions having overlapping biochemical effects, such as acetoacetate competing with the chloride anion for binding to an allosteric regulation site on the vesicular glutamate transporter [88], or acetoacetate, BHB, and butyrate all inhibiting class I HDACs in increasing order of potency[6]. Along these lines, it is of potential therapeutic interest that we found S-BHB to provide similar effects as the normal endogenous ketone body R-BHB. S-BHB is not a ketone body and is thought to be largely a low-abundance by-product of fatty acid oxidation. Due to the absolute specificity of BDH1 for R-BHB[66], S-BHB is oxidized only slowly and indirectly compared to R-BHB. However, as S-BHB shares most of the non-oxidative signaling properties ascribed to R-BHB[2], its slower oxidation translates to potentially more favorable pharmacokinetics than R-BHB as an exogenous signaling intervention. Many of the protein-binding effects of BHB may be relatively nonspecific, shared at varying potency by other small metabolic acids or anions. Understanding the systems biology effects of overlapping binding patterns of small metabolites, as well as the requirements for changes to the local or compartmental biochemical environment, are important areas for future investigation.

Both local and systemic factors may contribute to chronic neuroinflammation. We found positive correlations between liver weight, liver inflammatory gene expression, and brain inflammatory gene expression. These could represent parallel effects of Cyclic KD on liver and brain inflammation, that the inhibition of liver inflammation by long-term Cyclic KD modifies the systemic inflammatory environment, or both—that Cyclic KD both mitigates this source of systemic inflammation and modulates the response of microglia to systemic inflammatory cues. The relative importance of systemic versus local effects on chronic neuroinflammation is an important area for future studies to guide therapeutic development.

Strengths of our approach include leveraging a long-term KD mouse cohort run in parallel with lifespan and healthspan studies, combining *in vivo* and *in vitro* experiments to ensure physiological relevance and enable mechanistic inquiry, using multiple species and cell types for *in vitro* experiments, using a variety of compounds, and carefully attending to biochemical conditions. The experiments did use specific diet formulations, feeding durations and patterns, mouse strains, and *in vitro* inflammation models that inform constraints on the interpretation of our results.

Limitations of these data include the use of a single strain and sex in the long-term *in vivo* studies, limits of LPS as an *in vitro* model for age-related chronic inflammation, and the only partial overlap of BHB biology with KD biology. C57BL/6JN male mice from the NIA Aged Rodent Colony were used in the original lifespan study; this work is an extension of, for reasons previously described[15]. However, phenotypic differences between mouse sexes, strains, and substrains are well described[89,90], and these results should be validated in other mouse strains, such as the genetically heterogeneous UM-HET3 mice[91]. There is no established *in vitro* model for age-related chronic inflammation. LPS stimulation does not fully replicate the physiological changes associated with aging in our data, though microglia of varying ages do exhibit differential responses to LPS in mice[92]. Cellular senescence is tightly associated with age-induced chronic inflammation[93], so we employed this an alternative *in vitro* model. Further development and validation of *in vitro* models of age-related chronic inflammation will help advance research in this area. There is similarly no comprehensive, validated *in vitro* model for KD (or, e.g., fasting), and BHB is but one of multiple mechanisms involved in the inherently pleiotropic KD alongside the absence of carbohydrates and abundance of fatty acids. For example, an increase in γδ T cells and a p53-dependent form of cellular senescence by KD can occur independently of BHB and may involve changes in lipids or lipoproteins[11,14,94]. Feeding KD to animals, treating animals with BHB via exogenous ketones like 1,3-BD or ketone esters, and treating cells in culture with BHB are not synonymous. Even 1,3-BD has been reported to have BHB-independent effects[25]. The *in vivo* effects of exogenous ketones have been less well studied than KD, although 1,3-BD does increase lifespan in genetically heterogenous mice in the ITP[22,23]. A clearer understanding of the long-term effects on neuroinflammation of 1,3-BD, ketone esters, and other forms of exogenously administered subcomponents of KD biology will aid in developing the deeper mechanistic understanding that is required for successful translation of effects of KD into specific therapies for neuroinflammation.

In summary, our study demonstrates that 14-month Cyclic KD attenuates age-induced chronic inflammation in the brains of 26-month-old mice (**Fig. 1**), and the endogenous ketone metabolite R-BHB predominately attenuates LPS-induced inflammation in microglia *in vitro* (**Fig. 2**). This anti-inflammatory function is not dependent on the supply of energy, inhibition of HDACs, inhibition of the NLRP3 inflammasome, activation of HCAR2, or hnRNP A1 (**Fig. 3**).

An acidic environment induced by R-BHB may play a role (**Fig. 4**). These findings on neuroinflammatory modulation may help explain our prior results showing improvement in lifespan and memory function in aging mice fed Cyclic KD[15]. The results of our study indicate that intermittent exposure to KD or exogenous BHB may represent a promising dietary intervention for ameliorating chronic inflammation, a process that is widely regarded as a hallmark of the aging process[93,95].

Acknowledgments

This work was supported by the NIH grants R01AG067333 (J.C.N.), R01AG068025 (J.C.N.), T32AG000266 (M.N.), T32AG052374 (S.S.M. and B.E.), Buck intramural funds (J.C.N.), and University of Southern California Provost Fellowship Funding (S.S.M.). Both IMG and BV-2 cells were kindly provided by the Andersen Lab. Some illustrations were created with BioRender.com.

Authorship Contributions

M.N. conceived the studies, designed the experiments, analyzed experiments, and wrote the article. N.F.M., S.S.M., and W.C.M. analyzed the RNA-Seq data. T.Y.G., B.E., and C.G.A. helped with experiments. L.E. and D.F. provided important insights and suggestions to the article. E.V. supervised *in vivo* cohorts. J.C.N. supervised the full study and cowrote the article.

Conflicts of Interest

J.C.N. and E.V. are cofounders, stockholders, and coinventors on patents licensed to BHB Therapeutics, Ltd., and Selah Therapeutics Ltd., which develop ketone esters for consumer and therapeutic use.

Data Availability Statement

Raw datasets for RNA-Seq are deposited in GEO (GSE253612, GSE252513).

Supplementary Materials

Supplemental information can be found here: Supplementary.

References

1. Cahill G.F. (2006). Fuel metabolism in starvation. *Annu. Rev. Nutr.* **26**(1), 1–22. PMID: 16848698; doi: 10.1146/annurev.nutr.26.061505.111258.
2. Newman J.C. & Verdin E. (2017). β-Hydroxybutyrate: A signaling metabolite. *Annu. Rev. Nutr.* **37**(1), 51–76. PMID: 28826372; doi: 10.1146/annurev-nutr-071816-064916.
3. Puchalska P. & Crawford P.A. (2021). Metabolic and signaling roles of ketone bodies in health and disease. *Annu. Rev. Nutr.* **41**(1), 49–77. PMID: 34633859; doi: 10.1146/annurev-nutr-111120-111518.
4. Youm Y.H., Nguyen K.Y., Grant R.W., Goldberg E.L., Bodogai M., Kim D., … Dixit V.D. (2015). The ketone metabolite β-hydroxybutyrate blocks NLRP3 inflammasome-mediated inflammatory disease. *Nat. Med.* **21**(3), 263–269. PMID: 25686106; doi: 10.1038/nm.3804.
5. Goldberg E.L., Asher J.L., Molony R.D., Shaw A.C., Zeiss C.J., Wang C., … Dixit V.D. (2017). β-hydroxybutyrate deactivates neutrophil NLRP3 inflammasome to relieve gout flares. *Cell Rep.* **18**(9), 2077–2087. PMID: 28249154; doi: 10.1016/j.celrep.2017.02.004.
6. Shimazu T., Hirschey M.D., Newman J., He W., Shirakawa K., Le Moan N., … Verdin E. (2013). Suppression of oxidative stress by β-hydroxybutyrate, an endogenous histone deacetylase inhibitor. *Science* **339**(6116), 211–214. PMID: 23223453; doi: 10.1126/science.1227166.
7. Xie Z., Zhang D., Chung D., Tang Z., Huang H., Dai L., … Zhao Y. (2016). Metabolic regulation of gene expression by histone lysine β-hydroxybutyrylation. *Mol. Cell* **62**(2), 194–206. PMID: 27105115; doi: 10.1016/j.molcel.2016.03.036.
8. Taggart A.K.P., Kero J., Gan X., Cai T.Q., Cheng K., Ippolito M., … Waters M.G. (2005). (D)-beta-Hydroxybutyrate inhibits adipocyte lipolysis via the

nicotinic acid receptor PUMA-G. *J. Biol. Chem.* **280**(29), 26649–26652. PMID: 15929991; doi: 10.1074/jbc.C500213200.

9. Han Y.M., Bedarida T., Ding Y., Somba B.K., Lu Q., Wang Q., … Zou M.H. (2018). β-hydroxybutyrate prevents vascular senescence through hnRNP A1-mediated upregulation of Oct4. *Mol. Cell* **71**(6), 1064–1078.e5. PMID: 30197300; doi: 10.1016/j.molcel.2018.07.036.
10. Wang C.Y. & Liao J.K. (2012). A mouse model of diet-induced obesity and insulin resistance. *Methods Mol. Biol.* **821**, 421–433. PMID: 22125082; doi: 10.1007/978-1-61779-430-8_27.
11. Wei S.J., Schell J.R., Chocron E.S., Varmazyad M., Xu G., Chen W.H., … Gius D. (2024). Ketogenic diet induces p53-dependent cellular senescence in multiple organs. *Sci. Adv.* **10**(20), eado1463. PMID: 38758782; doi: 10.1126/sciadv.ado1463.
12. Lu J.F., Zhu M.Q., Xia B., Zhang N.N., Liu X.P., Liu H., … Wu J.W. (2023). GDF15 is a major determinant of ketogenic diet-induced weight loss. *Cell Metab.* **35**(12), 2165–2182.e7. PMID: 38056430; doi: 10.1016/j.cmet.2023.11.003.
13. Li X., Yang J., Zhou X., Dai C., Kong M., Xie L., … Hong S. (2024). Ketogenic diet-induced bile acids protect against obesity through reduced calorie absorption. *Nat. Metab.* **6**(7), 1397–1414. PMID: 38937659; doi: 10.1038/s42255-024-01072-1.
14. Goldberg E.L., Shchukina I., Asher J.L., Sidorov S., Artyomov M.N., & Dixit V.D. (2020). Ketogenesis activates metabolically protective γδ T cells in visceral adipose tissue. *Nat. Metab.* **2**(1), 50–61. PMID: 32694683; doi: 10.1038/s42255-019-0160-6.
15. Newman J.C., Covarrubias A.J., Zhao M., Yu X., Gut P., Ng C.P., … Verdin E. (2017). Ketogenic diet reduces midlife mortality and improves memory in aging mice. *Cell Metab.* **26**(3), 547–557.e8. PMID: 28877458; doi: 10.1016/j.cmet.2017.08.004.
16. Ang Q.Y., Alexander M., Newman J.C., Tian Y., Cai J., Upadhyay V., … Turnbaugh P.J. (2020). Ketogenic diets alter the gut microbiome resulting in decreased intestinal Th17 cells. *Cell* **181**(6), 1263–1275.e16. PMID: 32437658; doi: 10.1016/j.cell.2020.04.027.
17. Westerterp-Plantenga M.S., Nieuwenhuizen A., Tomé D., Soenen S., & Westerterp K.R. (2009) Dietary protein, weight loss, and weight maintenance. *Annu. Rev. Nutr.* **29**(1), 21–41. PMID: 19400750; doi: 10.1146/annurev-nutr-080508-141056.
18. Simpson S.J., Le Couteur D.G., Raubenheimer D., Solon-Biet S.M., Cooney G.J., Cogger V.C., & Fontana L. (2017). Dietary protein, aging and nutritional geometry. *Ageing Res. Rev.* **39**, 78–86. PMID: 28274839; doi: 10.1016/j.arr.2017.03.001.
19. Paoli A. (2014). Ketogenic diet for obesity: Friend or foe? *Int. J. Environ. Res. Public. Health* **11**(2), 2092–2107. PMID: 24557522; doi: 10.3390/ijerph110202092.
20. Roberts M.N., Wallace M.A., Tomilov A.A., Zhou Z., Marcotte G.R., Tran D., … Lopez-Dominguez J.A. (2017). A ketogenic diet extends longevity and healthspan in adult mice. *Cell Metab.* **26**(3), 539–546.e5. PMID: 28877457; doi: 10.1016/j.cmet.2017.08.005.
21. Tomita I., Tsuruta H., Yasuda-Yamahara M., Yamahara K., Kuwagata S., Tanaka-Sasaki Y., … Kume S. (2023). Ketone bodies: A double-edged sword for mammalian life span. *Aging Cell* **22**(6), e13833. PMID: 37060184; doi: 10.1111/acel.13833.
22. Jiang N., Gelfond J., Liu Q., Strong R., & Nelson J.F. (2024). The Gehan test identifies life-extending compounds overlooked by the log-rank test in the NIA Interventions Testing Program: Metformin, enalapril, caffeic acid phenethyl ester, green tea extract, and 17-dimethylaminoethylamino-17-demethoxygeldanamycin hydrochloride. *GeroScience* **46**(5), 4533–4541. PMID: 38630424; doi: 10.1007/s11357-024-01161-9.
23. Strong R., Miller R.A., Cheng C.J., Nelson J.F., Gelfond J., Allani S.K., … Harrison D.E. (2022). Lifespan benefits for the combination of rapamycin plus acarbose and for captopril in genetically heterogeneous mice. *Aging Cell* **21**(12), e13724. PMID: 36179270; doi: 10.1111/acel.13724.
24. Dowis K. & Banga S. (2021). The potential health benefits of the Ketogenic diet: A narrative review. *Nutrients* **13**(5), 1654. PMID: 34068325; doi: 10.3390/nu13051654.
25. McCarthy C.G., Waigi E.W., Yeoh B.S., Mell B., Vijay-Kumar M., Wenceslau C.F., & Joe B. (2022). Low-dose 1,3-butanediol reverses age-associated vascular dysfunction independent of ketone body β-hydroxybutyrate. *Am. J. Physiol. Heart Circ. Physiol.* **322**(3), H466–H473. PMID: 35148235; doi: 10.1152/ajpheart.00486.2021.
26. Papadopoli D., Boulay K., Kazak L., Pollak M., Mallette F., Topisirovic I., & Hulea L. (2019). mTOR as a central regulator of lifespan and aging. *F1000Res.* **8**: F1000 Faculty Rev-998. PMID: 31316753; doi: 10.12688/f1000research.17196.1.
27. López-Otín C., Blasco M.A., Partridge L., Serrano M., & Kroemer G. (2023). Hallmarks of aging: An expanding universe. *Cell* **186**(2), 243–278. PMID: 36599349; doi: 10.1016/j.cell.2022.11.001.
28. Selvarani R., Mohammed S., & Richardson A. (2021). Effect of rapamycin on aging and age-related diseases-past and future. *GeroScience* **43**(3), 1135–1158. PMID: 33037985; doi: 10.1007/s11357-020-00274-1.
29. Dobin A., Davis C.A., Schlesinger F., Drenkow J., Zaleski C., Jha S., … Gingeras T.R. (2013). STAR: Ultrafast universal RNA-Seq aligner. *Bioinformatics* **29**(1), 15–21. PMID: 23104886; doi: 10.1093/bioinformatics/bts635.
30. Bolger A.M., Lohse M., & Usadel B. (2014). Trimmomatic: A flexible trimmer for Illumina sequence data. *Bioinformatics* **30**(15), 2114–2120. PMID: 24695404; doi: 10.1093/bioinformatics/btu170.
31. Li B. & Dewey C.N. (2011). RSEM: Accurate transcript quantification from RNA-Seq data with or without a reference genome. *BMC Bioinformatics* **12**(1), 323. PMID: 21816040; doi: 10.1186/1471-2105-12-323.
32. Love M.I., Huber W., & Anders S. (2014). Moderated estimation of fold change and dispersion for RNA-Seq data with DESeq2. *Genome Biol.* **15**(12), 550. PMID: 25516281; doi: 10.1186/s13059-014-0550-8.
33. Mi H., Muruganujan A., Casagrande J.T., & Thomas P.D. (2013). Large-scale gene function analysis with the PANTHER classification system. *Nat. Protoc.* **8**(8), 1551–1566. PMID: 23868073; doi: 10.1038/nprot.2013.092.
34. Yu G., Wang L.G., Han Y., & He Q.Y. (2012). clusterProfiler: An R package for comparing biological themes among gene clusters. *OMICS* **16**(5), 284–287. PMID: 22455463; doi: 10.1089/omi.2011.0118.
35. Wu T., Hu E., Xu S., Chen M., Guo P., Dai Z., … Yu G. (2021). clusterProfiler 4.0: A universal enrichment tool for interpreting omics data. *Innovation (Camb)* **2**(3), 100141. PMID: 34557778; doi: 10.1016/j.xinn.2021.100141.
36. Yu G., Wang L.G., Yan G.R., & He Q.Y. (2015). DOSE: An R/Bioconductor package for disease ontology semantic and enrichment analysis. *Bioinformatics* **31**(4), 608–609. PMID: 25677125; doi: 10.1093/bioinformatics/btu684.
37. Carlson M. (2017). org.Hs.eg.db [Internet]. *Bioconductor*. Retrieved from https://bioconductor.org/packages/org.Hs.eg.db (accessed 24 October 2023).
38. Carlson M. (2017). org.Mm.eg.db [Internet]. *Bioconductor*. Retrieved from https://bioconductor.org/packages/org.Mm.eg.db (accessed 24 October 2023).
39. Wickham H. (2016). *ggplot2: Elegant Graphics for Data Analysis*. 2nd ed. Cham, Switzerland: Springer International Publishing.
40. Subramanian A., Tamayo P., Mootha V.K., Mukherjee S., Ebert B.L., Gillette M.A., … Mesirov J.P. (2005). Gene set enrichment analysis: A knowledge-based approach for interpreting genome-wide expression profiles. *Proc. Natl. Acad. Sci. U. S. A.* **102**(43), 15545–15550. PMID: 16199517; doi: 10.1073/pnas.0506580102.
41. Liberzon A., Birger C., Thorvaldsdóttir H., Ghandi M., Mesirov J.P., & Tamayo P. (2015). The Molecular Signatures Database (MSigDB) hallmark gene set collection. *Cell Syst.* **1**(6), 417–425. PMID: 26771021; doi: 10.1016/j.cels.2015.12.004.
42. Harris M.A., Clark J., Ireland A., Lomax J., Ashburner M., Foulger R., … Gene Ontology Consortium. (2004). The Gene Ontology (GO) database and informatics resource. *Nucleic Acids Res.* **32**(Suppl 1), D258–261. PMID: 14681407; doi: 10.1093/nar/gkh036.
43. Kanehisa M., Furumichi M., Tanabe M., Sato Y., & Morishima K. (2017). KEGG: New perspectives on genomes, pathways, diseases and drugs. *Nucleic Acids Res.* **45**(D1), D353–D361. PMID: 27899662; doi: 10.1093/nar/gkw1092.

44. Cahill K.M., Huo Z., Tseng G.C., Logan R.W., & Seney M.L. (2018). Improved identification of concordant and discordant gene expression signatures using an updated rank-rank hypergeometric overlap approach. *Sci. Rep.* **8**(1), 9588. PMID: 29942049; doi: 10.1038/s41598-018-27903-2.

45. Newman A.M., Steen C.B., Liu C.L., Gentles A.J., Chaudhuri A.A., Scherer F., … Alizadeh A.A. (2019). Determining cell type abundance and expression from bulk tissues with digital cytometry. *Nat. Biotechnol.* **37**(7), 773–782. PMID: 31061481; doi: 10.1038/s41587-019-0114-2.

46. Ogrodnik M., Evans S.A., Fielder E., Victorelli S., Kruger P., Salmonowicz H., … Jurk D. (2021). Whole-body senescent cell clearance alleviates age-related brain inflammation and cognitive impairment in mice. *Aging Cell* **20**(2), e13296. PMID: 33470505; doi: 10.1111/acel.13296.

47. Wolf F.A., Angerer P., & Theis F.J. (2018). SCANPY: Large-scale single-cell gene expression data analysis. *Genome Biol.* **19**(1), 15. PMID: 29409532; doi: 10.1186/s13059-017-1382-0.

48. Lian H., Roy E., & Zheng H. (2016). Protocol for primary microglial culture preparation. *Bio. Protoc.* **6**(21), e1989. PMID: 29104890; doi: 10.21769/BioProtoc.1989.

49. Toda G., Yamauchi T., Kadowaki T., & Ueki K. (2021). Preparation and culture of bone marrow-derived macrophages from mice for functional analysis. *STAR Protoc.* **2**(1), 100246. PMID: 33458708; doi: 10.1016/j.xpro.2020.100246.

50. Neri F., Basisty N., Desprez P.Y., Campisi J., & Schilling B. (2021). Quantitative proteomic analysis of the senescence-associated secretory phenotype by data-independent acquisition. *Curr. Protoc.* **1**(2), e32. PMID: 33524224; doi: 10.1002/cpz1.32.

51. Eap B., Nomura M., Panda O., Garcia T.Y., King C.D., Rose J.P., … Newman J.C. (2022). Ketone body metabolism declines with age in mice in a sex-dependent manner [Internet]. *BioRxiv*. doi: 10.1101/2022.10.05.511032 (accessed 2 December 2024).

52. Rahman M., Muhammad S., Khan M.A., Chen H., Ridder D.A., Müller-Fielitz H., … Schwaninger M. (2014). The β-hydroxybutyrate receptor HCA2 activates a neuroprotective subset of macrophages. *Nat. Commun.* **5**(1), 3944. PMID: 24845831; doi: 10.1038/ncomms4944.

53. Hirschberger S., Strauß G., Effinger D., Marstaller X., Ferstl A., Müller M.B., … Kreth S. (2021). Very-low-carbohydrate diet enhances human T-cell immunity through immunometabolic reprogramming. *EMBO Mol. Med.* **13**(8), e14323. PMID: 34151532; doi: 10.15252/emmm.202114323.

54. Karagiannis F., Peukert K., Surace L., Michla M., Nikolka F., Fox M., … Wilhelm C. (2022). Impaired ketogenesis ties metabolism to T cell dysfunction in COVID-19. *Nature* **609**(7928), 801–807. PMID: 35901960; doi: 10.1038/s41586-022-05128-8.

55. Luda K.M., Longo J., Kitchen-Goosen S.M., Duimstra L.R., Ma E.H., Watson M.J., … Jones R.G. (2023). Ketolysis drives CD8+ T cell effector function through effects on histone acetylation. *Immunity* **56**(9), 2021–2035.e8. PMID: 37516105; doi: 10.1016/j.immuni.2023.07.002.

56. Garrido-Rodríguez V., Herrero-Fernández I., Castro M.J., Castillo A., Rosado-Sánchez I., Galvá M.I., … Pacheco Y.M. (2021). Immunological features beyond CD4/CD8 ratio values in older individuals. *Aging (Albany, NY)* **13**(10), 13443–13459. PMID: 34038386; doi: 10.18632/aging.203109.

57. Mattson M.P. & Arumugam T.V. (2018). Hallmarks of brain aging: Adaptive and pathological modification by metabolic states. *Cell Metab.* **27**(6), 1176–1199. PMID: 29874566; doi: 10.1016/j.cmet.2018.05.011.

58. Wilson D.M., Cookson M.R., Van Den Bosch L., Zetterberg H., Holtzman D.M., & Dewachter I. (2023). Hallmarks of neurodegenerative diseases. *Cell* **186**(4), 693–714. PMID: 36803602; doi: 10.1016/j.cell.2022.12.032.

59. Allen W.E., Blosser T.R., Sullivan Z.A., Dulac C., & Zhuang X. (2023). Molecular and spatial signatures of mouse brain aging at single-cell resolution. *Cell* **186**(1), 194–208.e18. PMID: 36580914; doi: 10.1016/j.cell.2022.12.010.

60. Norden D.M. & Godbout J.P. (2013). Review: Microglia of the aged brain: Primed to be activated and resistant to regulation. *Neuropathol. Appl. Neurobiol.* **39**(1), 19–34. PMID: 23039106; doi: 10.1111/j.1365-2990.2012.01306.x.

61. Benito A., Hajji N., O'Neill K., Keun H.C., & Syed N. (2020). β-hydroxybutyrate oxidation promotes the accumulation of immunometabolites in activated microglia cells. *Metabolites* **10**(9), 346. PMID: 32859120; doi: 10.3390/metabo10090346.

62. Huang C., Wang P., Xu X., Zhang Y., Gong Y., Hu W., … Zhang W. (2018). The ketone body metabolite β-hydroxybutyrate induces an antidepression-associated ramification of microglia via HDACs inhibition-triggered Akt-small RhoGTPase activation. *Glia* **66**(2), 256–278. PMID: 29058362; doi: 10.1002/glia.23241.

63. Shippy D.C., Wilhelm C., Viharkumar P.A., Raife T.J., & Ulland T.K. (2020). β-Hydroxybutyrate inhibits inflammasome activation to attenuate Alzheimer's disease pathology. *J. Neuroinflammation* **17**(1), 280. PMID: 32958021; doi: 10.1186/s12974-020-01948-5.

64. Fu S.P., Wang J.F., Xue W.J., Liu H.M., Liu B.R., Zeng Y.L., … Liu J.X. (2015). Anti-inflammatory effects of BHBA in both *in vivo* and *in vitro* Parkinson's disease models are mediated by GPR109A-dependent mechanisms. *J. Neuroinflammation* **12**(1), 9. PMID: 25595674; doi: 10.1186/s12974-014-0230-3.

65. Candido E.P., Reeves R., & Davie J.R. (1978). Sodium butyrate inhibits histone deacetylation in cultured cells. *Cell* **14**(1), 105–113. PMID: 667927; doi: 10.1016/0092-8674(78)90305-7.

66. Green D.E., Dewan J.G., & Leloir L.F. (1937). The beta-hydroxybutyric dehydrogenase of animal tissues. *Biochem. J.* **31**(6), 934–949. PMID: 16746420; doi: 10.1042/bj0310934.

67. Webber R.J. & Edmond J. (1977). Utilization of L(+)-3-hydroxybutyrate, D(-)-3-hydroxybutyrate, acetoacetate, and glucose for respiration and lipid synthesis in the 18-day-old rat. *J. Biol. Chem.* **252**(15), 5222–5226. PMID: 885847; doi: 10.1016/S0021-9258(19)63335-1.

68. Wang Q.Q., Yin G., Huang J.R., Xi S.J., Qian F., Lee R.X., … Tang F.R. (2021). Ionizing radiation-induced brain cell aging and the potential underlying molecular mechanisms. *Cells* **10**(12), 3570. PMID: 34944078; doi: 10.3390/cells10123570.

69. Ng P.Y., McNeely T.L., & Baker D.J. (2023). Untangling senescent and damage-associated microglia in the aging and diseased brain. *FEBS J.* **290**(5), 1326–1339. PMID: 34873840; doi: 10.1111/febs.16315.

70. McCarthy R.C., Lu D.Y., Alkhateeb A., Gardeck A.M., Lee C.H., & Wessling-Resnick M. (2016). Characterization of a novel adult murine immortalized microglial cell line and its activation by amyloid-beta. *J. Neuroinflammation* **13**(1), 21. PMID: 26819091; doi: 10.1186/s12974-016-0484-z.

71. Blasi E., Barluzzi R., Bocchini V., Mazzolla R., & Bistoni F. (1990). Immortalization of murine microglial cells by a *v-raf/v-myc* carrying retrovirus. *J. Neuroimmunol* **27**(2–3), 229–237. PMID: 2110186; doi: 10.1016/0165-5728(90)90073-V.

72. Acuña-Catalán D., Shah S., Wehrfritz C., Nomura M., Acevedo A., Olmos C., … González-Billault C. (2024). Ketogenic diet administration later in life improves memory by modifying the synaptic cortical proteome via the PKA signaling pathway in aging mice. *Cell Rep. Med.* **5**(6), 101593. PMID: 38843842; doi: 10.1016/j.xcrm.2024.101593.

73. Enders J., Jack J., Thomas S., Lynch P., Lasnier S., Cao X., … Wright D.E. (2023). Ketolysis is required for the proper development and function of the somatosensory nervous system. *Exp. Neurol.* **365**, 114428. PMID: 37100111; doi: 10.1016/j.expneurol.2023.114428.

74. Marosi K., Kim S.W., Moehl K., Scheibye-Knudsen M., Cheng A., Cutler R., … Mattson M.P. (2016). 3-Hydroxybutyrate regulates energy metabolism and induces BDNF expression in cerebral cortical neurons. *J. Neurochem.* **139**(5), 769–781. PMID: 27739595; doi: 10.1111/jnc.13868.

75. Puchalska P., Martin S.E., Huang X., Lengfeld J.E., Daniel B., Graham M.J., … Crawford P.A. (2019). Hepatocyte-macrophage acetoacetate shuttle protects against tissue fibrosis. *Cell Metab.* **29**(2), 383–398.e7. PMID: 30449686; doi: 10.1016/j.cmet.2018.10.015.

76. Dai Y., Wei T., Shen Z., Bei Y., Lin H., & Dai H. (2021). Classical HDACs in the regulation of neuroinflammation. *Neurochem Int.* **150**, 105182. PMID: 34509559; doi: 10.1016/j.neuint.2021.105182.

77. Tsusaka T., Oses-Prieto J.A., Lee C., DeFelice B.C., Burlingame A.L., & Goldberg E.L. (2023). Non-specific recognition of histone modifications

by H3K9bhb antibody. *iScience* **26**(7), 107235. PMID: 37485368; doi: 10.1016/j.isci.2023.107235.

78. Li H., Wan X., Wu Z., Zhou Y., Chen R., Xu W., … Cen X. (2022). β-hydroxybutyrate reduces reinstatement of cocaine conditioned place preference through hippocampal CaMKII-α β-hydroxybutyrylation. *Cell Rep.* **41**(9), 111724. PMID: 36450263; doi: 10.1016/j.celrep.2022.111724.
79. Han W., Zhang B., Zhao W., Zhao W., He J., Qiu X., … Wang Z. (2024). Ketogenic β-hydroxybutyrate regulates β-hydroxybutyrylation of TCA cycle-associated enzymes and attenuates disease-associated pathologies in Alzheimer's mice. *Aging Cell* (ahead of print), e14368. PMID: 39411885; doi: 10.1111/acel.14368.
80. Koronowski K.B., Greco C.M., Huang H., Kim J.K., Fribourgh J.L., Crosby P., … Sassone-Corsi P. (2021). Ketogenesis impact on liver metabolism revealed by proteomics of lysine β-hydroxybutyrylation. *Cell Rep.* **36**(5), 109487. PMID: 34348140; doi: 10.1016/j.celrep.2021.109487.
81. Rajamäki K., Nordström T., Nurmi K., Åkerman K.E.O., Kovanen P.T., Öörni K., & Eklund K.K. (2013). Extracellular acidosis is a novel danger signal alerting innate immunity via the NLRP3 inflammasome. *J. Biol. Chem.* **288**(19), 13410–13419. PMID: 23530046; doi: 10.1074/jbc.M112.426254.
82. McCarthy C.G., Chakraborty S., Singh G., Yeoh B.S., Schreckenberger Z.J., Singh A., … Joe B. (2021). Ketone body β-hydroxybutyrate is an autophagy-dependent vasodilator. *JCI Insight* **6**(20), e149037. PMID: 34499623; doi: 10.1172/jci.insight.149037.
83. Moutinho M., Puntambekar S.S., Tsai A.P., Coronel I., Lin P.B., Casali B.T., … Landreth G.E. (2022). The niacin receptor HCAR2 modulates microglial response and limits disease progression in a mouse model of Alzheimer's disease. *Sci. Transl. Med.* **14**(637), eabl7634. PMID: 35320002; doi: 10.1126/scitranslmed.abl7634.
84. Zhao C., Wang H., Liu Y., Cheng L., Wang B., Tian X., … Shao Z. (2023). Biased allosteric activation of ketone body receptor HCAR2 suppresses inflammation. *Mol. Cell.* **83**(17), 3171–3187.e7. PMID: 37597514; doi: 10.1016/j.molcel.2023.07.030.
85. Singh N., Gurav A., Sivaprakasam S., Brady E., Padia R., Shi H., … Ganapathy V. (2014). Activation of Gpr109a, receptor for niacin and the commensal metabolite butyrate, suppresses colonic inflammation and carcinogenesis. *Immunity* **40**(1), 128–139. PMID: 24412617; doi: 10.1016/j.immuni.2013.12.007.
86. Arsyad A., Idris I., Rasyid A.A., Usman R.A., Faradillah K.R., Latif W.O.U., … Djabir Y.Y. (2020). Long-term ketogenic diet induces metabolic acidosis, anemia, and oxidative stress in healthy wistar rats. *J. Nutr. Metab.* **2020**(17), 3642035. PMID: 32685205; doi: 10.1155/2020/3642035.
87. Choudhary A., Mu C., Barrett K.T., Charkhand B., Williams-Dyjur C., Marks W.N., … Scantlebury M.H. (2021). The link between brain acidosis, breathing and seizures: A novel mechanism of action for the ketogenic diet in a model of infantile spasms. *Brain Commun.* **3**(4), fcab189. PMID: 34734183; doi: 10.1093/braincomms/fcab189.
88. Juge N., Gray J.A., Omote H., Miyaji T., Inoue T., Hara C., … Moriyama Y. (2010). Metabolic control of vesicular glutamate transport and release. *Neuron* **68**(1), 99–112. PMID: 20920794; doi: 10.1016/j.neuron.2010.09.002.
89. Montgomery M.K., Hallahan N.L., Brown S.H., Liu M., Mitchell T.W., Cooney G.J., & Turner N. (2013). Mouse strain-dependent variation in obesity and glucose homeostasis in response to high-fat feeding. *Diabetologia* **56**(5), 1129–1139. PMID: 23423668; doi: 10.1007/s00125-013-2846-8.
90. Mekada K. & Yoshiki A. (2021). Substrains matter in phenotyping of C57BL/6 mice. *Exp. Anim.* **70**(2), 145–160. PMID: 33441510; doi: 10.1538/expanim.20-0158.
91. Nadon N.L., Strong R., Miller R.A., & Harrison D.E. (2017). NIA Interventions Testing Program: Investigating putative aging intervention agents in a genetically heterogeneous mouse model. *EBioMedicine* **21**, 3–4. PMID: 27923560; doi: 10.1016/j.ebiom.2016.11.038.
92. Li X., Li Y., Jin Y., Zhang Y., Wu J., Xu Z., … Peng B. (2023). Transcriptional and epigenetic decoding of the microglial aging process. *Nat. Aging* **3**(10), 1288–1311. PMID: 37697166; doi: 10.1038/s43587-023-00479-x.
93. Baechle J.J., Chen N., Makhijani P., Winer S., Furman D., & Winer D.A. (2023). Chronic inflammation and the hallmarks of aging. *Mol. Metab.* **74**, 101755. PMID: 37329949; doi: 10.1016/j.molmet.2023.101755.
94. Goldberg E.L., Molony R.D., Kudo E., Sidorov S., Kong Y., Dixit V.D., & Iwasaki A. (2019). Ketogenic diet activates protective γδ T cell responses against influenza virus infection. *Sci. Immunol.* **4**(41), eaav2026. PMID: 31732517; doi: 10.1126/sciimmunol.aav2026.
95. Furman D., Campisi J., Verdin E., Carrera-Bastos P., Targ S., Franceschi C., Ferrucci L., … Slavich G.M. (2019). Chronic inflammation in the etiology of disease across the life span. *Nat. Med.* **25**(12), 1822–1832. PMID: 31806905; doi: 10.1038/s41591-019-0675-0.